SYNTHESIS OF MAGNETICALLY ANISOTROPIC JANUS PARTICLES BY DROPLET-BASED MICROFLUIDICS

A DISSERTATION SUBMITTED TO
THE GRADUATE SCHOOL OF ENGINEERING AND SCIENCE
OF BILKENT UNIVERSITY
IN PARTIAL FULFILLMENT OF THE REQUIREMENTS FOR
THE DEGREE OF
DOCTOR OF PHILOSOPHY
IN
MECHANICAL ENGINEERING

By
Muhammad Saqib
January 2024

SYNTHESIS OF MAGNETICALLY ANISOTROPIC JANUS PARTICLES BY DROPLET-BASED MICROFLUIDICS

By Muhammad Saqib

January 2024

We certify that we have read this dissertation and that in our opinion it is fully adequate, in scope and in quality, as a dissertation for the degree of Doctor of Philosophy.

E. Yegan Erdem(Advisor)

Luca Biancofiore

Selis Önel

Barbaros Çetin

Ali Koşar

Approved for the Graduate School of Engineering and Science:

Orhan Arıkan
Director of the Graduate School

ABSTRACT

SYNTHESIS OF MAGNETICALLY ANISOTROPIC JANUS PARTICLES BY DROPLET-BASED MICROFLUIDICS

Muhammad Saqib
Ph.D. in Mechanical Engineering
Advisor: E. Yegan Erdem
January 2024

In the past decade Janus particles have been extensively utilized by the scientific community for potential uses such as cell encapsulation and assembly, DNA assays, biological multiplexing , targeted drug delivery, noninvasive imaging, theranostics , microlenses, reflection-mode displays, removal of organic and metal pollutants and water decontamination. Due to their multi functional characteristics, stemming from their anisotropy, they are superior to conventional monophase particles. Even though there are several established synthesis methods for Janus particles, microfluidics-based methods are by far the most convenient and reliable due to low reagent consumption, monodispersity of the resultant particles and efficient control over reaction conditions. Droplet-based microfluidics is the most popular technique for the reliable synthesis of Janus particles and even though it has been extensively explored there are many aspects of the conventional droplet-based microfluidics techniques that either result in poor anisotropy of the synthesized particles or involve off-chip processing. In this work a simple and novel droplet-based microfluidic technique is utilized to synthesize magnetically anisotropic Janus particles. Using this method magnetically anisotropic Janus particles are synthesized by using droplets as templates. The droplets contain magnetic nanoparticles and are exposed to ultraviolet radiation while passing through a magnetic field. The magnetic field renders the droplet anisotropic by attracting the magnetic nanoparticles to one hemisphere while at the same time the ultrviolet exposure initiates polymerization of the prepolymer phase. The microfluidic device was optimized by using numerical simulations and experimental observations. The magnetic flux density was optimized by using a magnetic flux density map. The synthesized particles were imaged under an optical microscope to observe their size distribution and scanning electron microscope to confirm complete polymerization and the magnetic anisotropy was confirmed by observing the motion of the particle in the presence of an external magnetic field. The

synthesized particles were observed to be monodisperse and exhibited rotation about their own axis which is characteristic of magnetically anisotropic particles. Further another design was developed to merge droplets from two dispersed phase streams in a Janus orientation by optimizing the angle of merging. With this device the merged droplet was observed to contain the constituents of its two hemispheres distinct from each other. Using this device TiO_2-Fe_2O_3 and SiO_2-Fe_2O_3 magnetically anisotropic Janus particles were synthesized. The synthesized Janus particles were observed under the optical microscope and the scanning electron microscope. Moreover the magnetic response of the Janus particles was also observed using a permanent magnet. These types of Janus particles could be potentially used as micromotors for microcargo transport because of their magnetic properties or for DNA assay applications.

Keywords: janus, anisotropy, microfluidic, droplet-based.

ÖZET

DAMLALCIK TEMELLİ MİKROAKIŞKAN SİSTEMDE MANYETİK ÖZELLİKLİ ANİZOTROPİK JANUS PARÇACIKLARIN SENTEZİ

Muhammad Saqib
Makine Mühendisliği, Doktora
Tez Danışmanı: E. Yegan Erdem
Ocak 2024

Janus parçacıklar, son yıllarda araştırmacılar tarafından hücre işaretleme, DNA testleri, biyolojik çoğaltma, hedefli ilaç taşıma, görüntüleme, ekran teknolojisi, organik ve metal kirleticilerin uzaklaştırılması ve su arıtma gibi birçok amaç için kullanılmaktadır. Anizotropilerinden kaynaklanan çok fonksiyonlu özellikleri nedeniyle, konvansiyonel monofaz parçacıklara göre daha üstün özelliklere sahiptirler. Janus parçacıkların üretiminde kullanılan geleneksel sentez yöntemleri olmasına rağmen, mikroakışkan tabanlı sistemler, kontrollü malzeme tüketimi, bir örnek üretim ve reaksiyon koşulları üzerinde etkili kontrol nedeniyle konvansiyonel yöntemlere göre daha avantajlıdır. Damlacık tabanlı mikroakışkan sistemler, Janus parçacıkların güvenilir sentezi için en popüler tekniktir. Bu metot farklı sentezler için de kullanılıyor olup, literatürde yer alan çalışmaların çoğu Janus parçacıkların üretiminde üretim sonrası ek işlemleri gerektirmektedir. Bu çalışmada, manyetik anizotropik Janus parçacıkların sentezlenmesi için basit ve yenilikçi bir damlacık tabanlı mikroakışkan teknik kullanılmıştır. Bu yöntemle, manyetik anizotropik Janus parçacıklar, damlaların şablon olarak kullanılmasıyla sentezlenir. Damlalar, manyetik nanoparçacıklar içerir ve manyetik bir alan içinden geçerken ultraviyole ışına maruz bırakılır. Manyetik alan, manyetik nanoparçacıkları bir yarımküreye çekerek damlayı anizotropik hale getirirken, aynı anda ultraviyole maruziyeti ön polimer fazının polimerizasyonunu başlatır. Bu tezde geliştirilen mikroakışkan sistem, sayısal simülasyonlar ve deneysel gözlemler kullanılarak optimize edilmiştir. Manyetik alan yoğunluğu optimize edilmiştir. Sentezlenen parçacıklar, optik mikroskop altında boyut dağılımlarını gözlemlemek ve tam polimerizasyonu doğrulamak için taramalı elektron mikroskop altında görüntülenmiş; manyetik anizotropi, dış bir manyetik alanın varlığında partikülün hareketini gözlemleyerek doğrulanmıştır. Sentezlenen parçacıkların birörnek olduğu ve kendi ekseni etrafında dönme özelliği

gösterdiği gözlemlenmiştir, bu da manyetik anizotropik parçacıkların karakteristik özelliğidir. Bu tez kapsamında iki farklı nanoparçacık türünün yer aldığı Janus parçacıkların sentezi için de yenilikçi mikroakışkan sistemler geliştirilmiştir. Bu sistemlerde TiO2-Fe3O4 ve SiO2-Fe3O4 nanoparçacıklarından oluşan manyetik anizotropik Janus parçacıkları sentezlenmiştir. Sentezlenen Janus parçacıklar, optik mikroskop ve taramalı elektron mikroskop altında gözlemlenmiştir. Ayrıca Janus parçacıkların manyetik tepkisi kalıcı mıknatıs kullanılarak da test edilmiştir. Bu tür Janus parçacıklar manyetik özellikleri sayesinde mikro kargo taşıma veya DNA testi uygulamaları için kullanılabilecektir.

Anahtar sözcükler: janus, anizotropi, mikrofluidik, damlalı-tabanlı.

Acknowledgement

In the name of Allaah, the only Creator of all that exists. All praise and thanks to Allaah for granting me the ability to complete this thesis.

First and foremost I would like to thank my research advisor Dr. Yegan Erdem for her continuous guidance, support and cooperation throughout the period of my PhD program in the form of sharing her technical expertise, her laboratory experience and in the form of including me in the esteemed project that I had the privilege of working on. I would like to additionally thank her for her patience, support and invaluable input and feedback into my research specifically her input and feedback for our conference and journal papers. I would also like to thank the thesis tracking committee members Dr. Selis Önel and Dr. Luca Biancofiore for their valuable suggestions and input throughout the duratıon of my PhD. I would also like to thank Dr. Barbaros Çetin and Dr. Ali Koşar for examining my thesis and for their valuable feedback and suggestions.

I also would like to extend my heartfelt gratitude to Dr. Batur Ercan for his wonderful suggestions and input regarding my experiments and his contribution in the manuscripts we wrote together.

I would like to take this opportunity to thank the technical staff at UNAM specially Mr. Abdullah Kafadenk, Mr. Taha Ilikkan and Mr. Semih Bozkurt for their assistance with training of the equipment and for their help with the fabrication procedure for my microfluidic devices. Also Dr. Gunes Kibar for her help with my experiments.

I would like to acknowledge the support and care from my family, specially my father, my mother, my sister Anum and my brother Hamza throughout my stay in Bilkent University. Without their love, care and invaluable support I would not have been able to pursue and complete my higher education in Turkey. My wife Javaria was with me throughout this journey and her support and company is something without which I would not have been able to get through this and I love her for that. And I also love her for being a wonderful mother to our beautiful son Musa whose smile made me forget all my worries and stress.

I would like to thank my grandfather by relation Dr. Ahmet bahtiyar Eşref and his family Chacha Mana and Shabnam Khala for being a family to us during

my stay in Turkey.

Last but not the least I would like to thank my group members, office colleagues and neighbors Humayun Ahmed, Sayed us Salehin, Atif Ali, Abdus Salam, Vahit Çorumlu, Osman Berkay Sahinoglu, Naveed Mahmood and Hamza Humayun for their keeping me company.

Contents

List of Figures

List of Tables

Chapter 1

Introduction

Synthesis of micro particles having multifunctional properties has become a growing field of scientific research over the past several years because of their unique physical properties as a result of the high surface to volume ratio. Moreover there is a category of particles that display different physical and chemical properties in different orientations. This phenomenon is called anisotropy. In comparison to conventional microparticles, anisotropic microparticles exhibit hybrid characteristics providing several advantages in various applications like cell encapsulation and assembly [1], DNA assays [2], biological multiplexing [3], targeted drug delivery [4–9], noninvasive imaging [10], theranostics [11, 12], microlenses [13–15], reflection-mode displays [16], removal of organic and metal pollutants [17,18], and water decontamination [19,20]. Anisotropic particles are more commonly referred to as Janus particles due to their dual characteristics. Since Janus particles can be potentially employed in such a wide variety of applications, several methods have been reported for the synthesis of these particles. Categorized broadly, the synthesis techniques are of two types: batch wise synthesis techniques and microfluidic-based techniques. Under the batch wise category, Janus particles are generally synthesized *via* masking, phase separation and self-assembly techniques [21]. In the masking technique certain regions of the substrate are protected from chemical/physical modification while other regions are not protected and thus undergo the required chemical/physical changes [22]. The chemical/physical modifications

in case of this method are brought about *via* etching, deposition, ion implantation, or annealing processes. The phase separation technique is based on the principle that when a polymer solution is mixed with a precursor, the mixture tends to separate into distinct phases due to differences in solubility and miscibility. This separation process is optimized by controlling physical factors like temperature, concentration, and material properties [23]. Finally cross-linking is performed to lock the polymer phases in place. The principle behind self-assembly is that certain particles can arrange into certain organized structures due to a number of physical or chemical interactions, like van der Waals forces, electrostatic interactions, hydrogen bonding, and others. The process is initiated by dispersing block copolymers in a solvent and later the block copolymers are assembled through solvent exchange and finally the core is cross-linked to obtain anisotropic particles [24].

Although these batch wise synthesis techniques are promising, they have inherent disadvantages that limit their applicability, like polydispersity, limited control over reactions conditions, and wasteful consumption of reagents [25]. In contrast microfluidic-based techniques provide superior control over reaction conditions, narrow size distribution of synthesized particles and minimal consumption of reagents [26]. Microfluidics is a multidisciplinary field that involves manipulation of fluids at a micro/nano scale. Microfluidics allows precise control over the reaction conditions and efficient transfer of heat into and out of the system due to the small size of the microreactor. There are two types of microfluidics reactors; continuous and droplet-based. In continuous type microfluidics, the fluid is driven inside the microchannels by pressure driven flow or electro-osmotic flow. Continuous type flow has a parabolic flow profile which develops as a result of the no-slip boundary condition at the wall. There is dispersion at the walls which causes fluid at the wall to be slower than the fluid in the center of the channel. This leads to non-uniform resident time inside the microchannels which is not desirable in all the applications especially chemical syntheses and biological analyses [27, 28]. Furthermore unless there is a stimulus to enhance mixing, parallel flowing fluids do not diffuse into each other before the characteristic diffusion length which depends on the microchannel geometry [29].

Moreover droplet-based microfluidics allows rapid mixing due to the chaotic advection as a result of the the recirculation zones produced by the two phase flow inside a microchannel [30]. Droplets in a microfluidic system act as individual microreactors that can be used to perform reactions with higher efficiency as compared to non-droplet based (continuous) microfluidic systems [31]. For these reasons microfluidic droplet-based synthesis techniques have gained popularity not only for isotropic particles but also for Janus particle synthesis [32]. There are several microfluidic-based techniques for the synthesis of Janus particles reported in the literature that can be broadly classified into four categories namely co-flowing streams, phase separation, double-emulsion, and electrohydrodynamic co-jetting [33].

1.1 Co-Flowing Streams

The co-flowing streams method depends on the fact that fluids with varying chemical/physical compositions can flow parallel to one another without dispersing into each other until a characteristic dispersion length. This is caused by the viscous forces that hinder diffusion. The synthesis methods in this category take advantage of this diffusion length and the co-flowing stream is sheared into droplets by a continuous phase generally in a flow-focusing configuration. Afterwards these droplets are polymerized by UV exposure [34, 35], thermal curing [3] or ionic crosslinking [36,37] to produce solid particles with two hemispheres of different compositions. There are two types of fluid systems in a co-flowing method; miscible or immiscible. In case of miscible streams the viscosities and the velocities of the two co-flowing fluids need to match in order to avoid mixing [38], whereas in case of immiscible stream the Janus droplet generation is governed by the spreading coefficient [39].

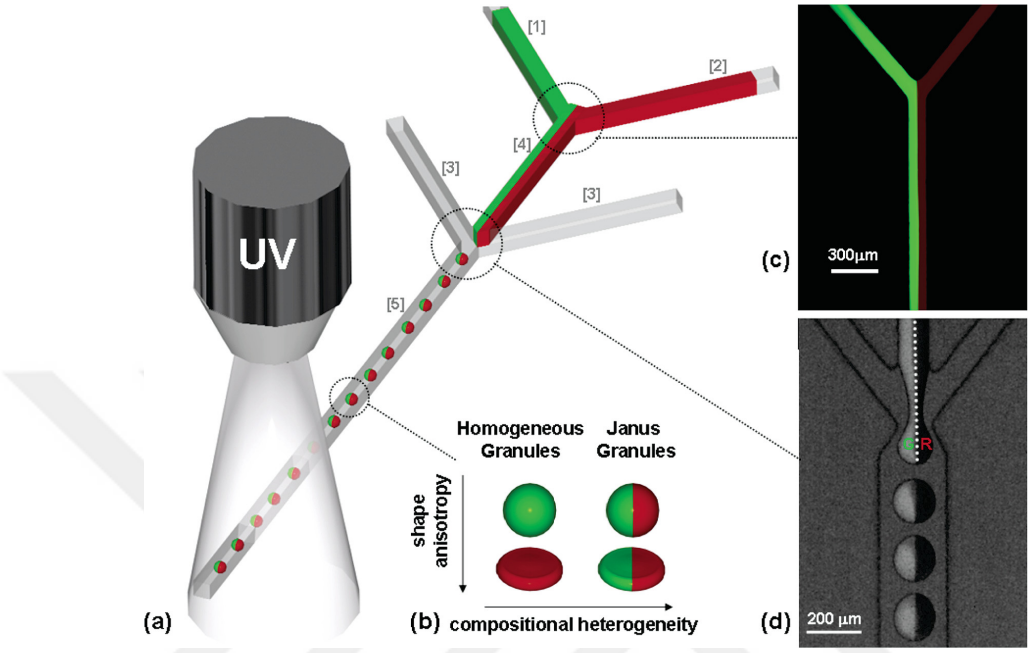

Figure 1.1: Schematic of the co-flow device that has been utilized in literature for the synthesis of Janus particles. Note: Reprinted with permission from Shepherd RF, Conrad JC, Rhodes SK, *et al.* Microfluidic assembly of homogeneous and janus colloid-filled hydrogel granules. Langmuir. 2006,22(21),8618–8622. Copyright (2006) American Chemical Society [40].

1.1.1 Miscible Streams

Flow in microfluidics-based devices is laminar predominantly due to the small length scales. At this small length scale, two parallel flowing fluids do not mix completely with each other until a certain characteristic diffusion length. Therefore, while keeping the velocities and the viscosities of the two parallel flowing streams same, a microfluidic droplet generator is utilized to generate Janus droplets in which a clear interface is maintained between the two hemispheres. The maintenance of a clear interface after droplet generation is dependent on the production of symmetric recirculation zones that are generated because of the two phase flow and are produced symmetrically along the direction of the flow. Several research groups have reported techniques based on this principle to synthesize Janus particles having anisotropies such as amphiphilicity [5], optical anisotropy [41, 42], and magnetic anisotropy [43, 44]. Nisisako *et al.* [45]

demonstrated the fabrication of dual coloured microspheres using this method by performing off-chip thermal curing. Further breakthroughs in this category were reported by Shepherd *et al.* [40] as they described the synthesis of spherical and discoidal shaped Janus hydrogel granules by changing the cross-sectional configuration of the microchannels. The schematic of their synthesis technique is shown in Figure 1.1. Seiffert *et al.* [46] reported the synthesis of Janus microshells (hollow) using a non-polymerizable phase as the middle stream and two polymerizable outer co-flowing streams. The synthesized microspheres were washed to remove the middle core which caused the non-polymerizable phase to be removed and therefore made the microspheres hollow. Another novel approach to produce multienzymatic microreactors exhibiting magnetic anisotropy was reported by Kamperman *et al.* [47] utilizing in-air microfluidics. In the case of in-air microfluidics the co-flowing streams are transported in air instead of a traditional continuous phase fluid. The produced droplets were cured by a cross-linking jet showered at them as they were generated. According to this study in-air microfluidics approach increased the production rate by two to three orders of magnitude in comparison to the conventional microfluidic approach. An emulsion-based external gelation method was reported by Zhao *et al.* [44] to synthesize magnetically anisotropic hydrogel microparticles. The technique consisted of droplet generation of a co-flowing stream, in which one stream contained sodium alginate solution and the other contained a mixture of sodium alginate solution and magnetic nanoparticles, followed by the cross-linking of the Janus droplets by means of encapsulation in a larger $CaCl_2$ droplet generated downstream. Although this method produced magnetically anisotropic particles, the size and shape of the particles was non-uniform. As an improvement to this method Liu *et al.* [48] demonstrated the synthesis of hydrogel microparticles having magnetic anisotropy *via* a continuous stream of $CaCl_2$ instead of droplets. By making this modification it was reported that the shape and size distribution of the magnetic Janus particles were improved significantly.

The co-flow method exploits the ability of two parallel flowing fluids to flow without merging for the length of the diffusion scale. In spite of that the requirement for the viscosities and the velocities of the co-flowing fluids to be identical

limits the use of this technique greatly [2, 3].

1.1.2 Immiscible Streams

The second category of co-flowing streams method is the case where the two parallel flowing phases are immiscible. For such cases the form of the Janus particles depends on the spreading coefficient. The spreading coefficient S is given by:

$$S = \gamma_{PQ} - (\gamma_P + \gamma_Q) \tag{1.1}$$

where γ_{PQ} is the interfacial tension between the two parallel flowing phases, γ_P is the interfacial tension between the co-flowing phase P and continuous phase fluid, and γ_Q is the interfacial tension between the co-flowing phase Q and continuous phase fluid [49, 50].

There are three possibilities for such a three fluid system which contains two immiscible liquids (P,Q) immersed in one host liquid.

- **Complete engulfing**: This is the case when one droplet phase completely engulfs the other droplet phase. This happens when $\gamma_P > (\gamma_Q + \gamma_{PQ})$ or $\gamma_Q > (\gamma_P + \gamma_{PQ})$
- **Non-engulfing**: This is the case when the two droplet phases stay separated. This happens when $\gamma_{PQ} > (\gamma_P + \gamma_Q)$.
- **Partial engulfing**: This is the case when droplets stay in the Janus orientation. In this case both dispersed phases have a common interface.

One of the earliest examples of the use of this technique is the study by Nisisako *et al.* [36] where they reported the synthesis of truncated Janus particles by using one polymerizable and one non-polymerizable fluid as the co-flowing fluids. The

generated droplets were collected and off-chip UV curing was performed to solidify them, after which the non-polymerizable phase was removed *via* washing and truncated Janus particles were produced which could be shape tuned by varying the interfacial tension between the two co-flowing phases. This technique has been utilized by other researchers to synthesize truncated, crescent and hollow shaped anisotropic supraparticles for use in novel color displays [34]. This technique has been used for the fabrication of biconvex and biconcave microlenses by keeping one of the phases as non-polymerizable [14, 15]. By controlled decoration of Ag nanoparticles on the concave surface of the Janus particle, TiO_2 nanoparticles on the convex surface and magnetic nanoparticles in the core, Chen *et al.* [19] demonstrated the use of Janus particles for water decontamination applications. Prasad *et al.* [51] implemented a co-flowing system with immiscible monomers to synthesize dumbbell or snowman shaped magnetically anisotropic Janus particles. The shape of the particles was determined by the capillary number of the co-flowing streams.

Yang *et al.* [52] reported a side-by-side capillary device for the synthesis of anisotropic Janus particles in which the magnetic anisotropy was dependent on the immiscibility of the co-flowing streams. Xu *et al.* [53] utilized a selectively surface modified microfluidic device for the synthesis of Janus particles. The surface modification of the microchannels was performed in such a way that one half of the channel was rendered hydrophobic along the entire length and the other half was rendered hydrophilic in the same manner. Due to this surface modification the dispersed phase, which was a combination of parallel flowing streams of a hydrophobic and a hydrophilic monomer, flowed inside the microchannel in a way that the hydrophilic monomer flowed along the hydrophilic part of the channel while the hydrophobic monomer flowed along the hydrophobic part of the channel. Later droplet generation followed by UV polymerization was performed to produce amphiphilic particles.

Although this method provides better compartmentalization compared to the miscible streams method, non-uniformity in particle shape is a drawback that creates difficulty in repeatability of the results [4].

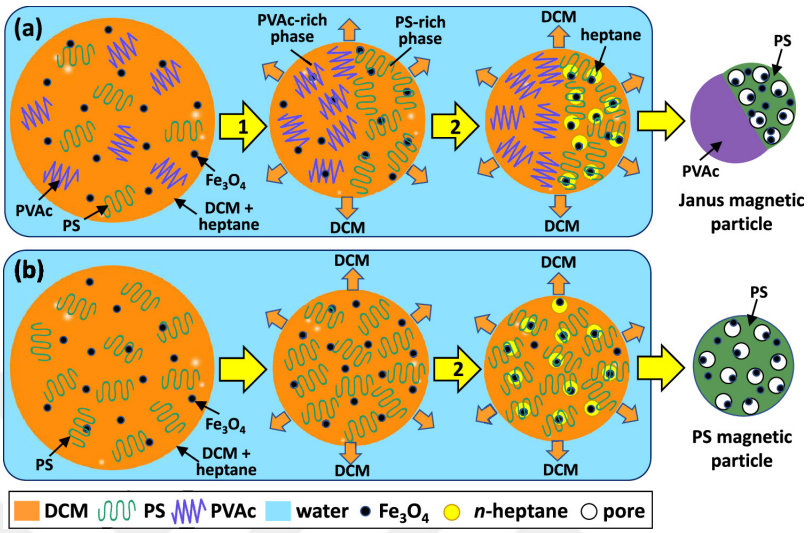

Figure 1.2: Schematic of the phase separation method that has been utilized in literature for the synthesis of Janus particles. Note: Reprinted with permission from Al Nuumani R, Smoukov SK, Bolognesi G, *et al.* Highly porous magnetic Janus microparticles with asymmetric surface topology. Langmuir. 2020;36(42):12702–12711. Copyright 2020 American Chemical Society [54].

1.2 Phase separation

The phase separation method does not require precise control over flow parameters to maintain the interface between the two halves of the Janus particles. Unlike the co-flow method, the phase separation method is based on the principle that different monomers react differently to heat energy absorption depending on their chemical properties [55, 56]. The first implementation of the phase separation method for Janus particle synthesis was achieved by Shah *et al.* [57] in which they produced microparticles with one side made out of hydrogel and the other side comprising primarily of aggregated colloidal nanoparticles. The method was a two-step phase separation process, with heat-induced shrinkage and accumulation of microgels to one hemisphere being the first step and UV polymerization of acrylamide monomer in the second hemisphere being the final step. The final product was magnetically anisotropic Janus particles. Lone *et al.* [58] synthesized Janus particles with a protruding head *via* a UV-directed phase separation. Another novel technique that utilized the difference in the rates of phase separation and UV polymerization between the two hemispheres

of the generated droplet to produce asymmetric porous Janus particles was reported by Kim *et al.* [59]. The surface anisotropy of the particles was achieved by exposing one side of the droplets to UV radiation and blocking the UV from reaching the other side. Due to this difference in UV exposure, the particle side exposed to UV swelled and wrinkled when dried, whereas the UV blocked side remained smooth, and hence, the particle became asymmetrically porous. Li *et al.* [60] achieved a morphology transition from core-shell microcapsule to Janus by altering the nature of the dispersed phase from an organochloride to an organic fluid. Jeong *et al.* [55] synthesized magnetically anisotropic Janus particles by using a mixture of incompatible monomers. After the droplet generation, the droplets were provided heat due to which the solvent in the droplets evaporated and the incompatible monomers segregated into two sections rendering the particles anisotropic. Ekanem *et al.* [61] produced patchy Janus particles by a phase separation method. They concluded that the extent of patches on the particles was dependent on the size of the droplets. Smaller droplets required a shorter solidification time and therefore underwent incomplete phase separation while larger droplets required a higher solidification time and therefore underwent complete phase separation resulting in no patches on particles. Wang *et al.* [62] reported an off-chip magnetically driven phase separation method for the production of magnetically anisotropic amphiphilic Janus particles. Sun *et al.* [63] designed a flow-focusing droplet generator coupled with a serpentine channel for synthesizing Janus-patchy, triple, quadruple and core-shell type particles by varying the amount and type of surfactant added to the dispersed phase. Xia *et al.* [64] demonstrated that the difference in density of particles suspended in a droplet leads to different shapes of the synthesized Janus particles. They concluded that low-density nanoparticles resulted in a more spherical and high-density nanoparticles resulted in a flattened shape of the Janus particles. Ren *et al.* [20] synthesized crescent-shaped Janus particles *via* a solvent loss based phase separation method for potential use in water decontamination applications. The particles had iron oxide magnetic nanoparticles on the convex surface and manganese oxide nanoparticles on the concave surface to act as micromotors. Another example of an off-chip solvent evaporation-based phase separation method to synthesize

Janus particles is the work of Al Nuumani *et al.* [54] in which they synthesize particles that are porous on one hemisphere and non-porous on the other hemisphere. The schematic of their synthesis technique is shown in Figure 1.2.

Even though phase separation is a versatile technique to synthesize Janus particles its limitation to produce particles with narrow size distribution, which stems from the fact that different blends of polymers are used inside the prepolymer phase, makes it unsuitable for the synthesis of large amounts of Janus structures [56].

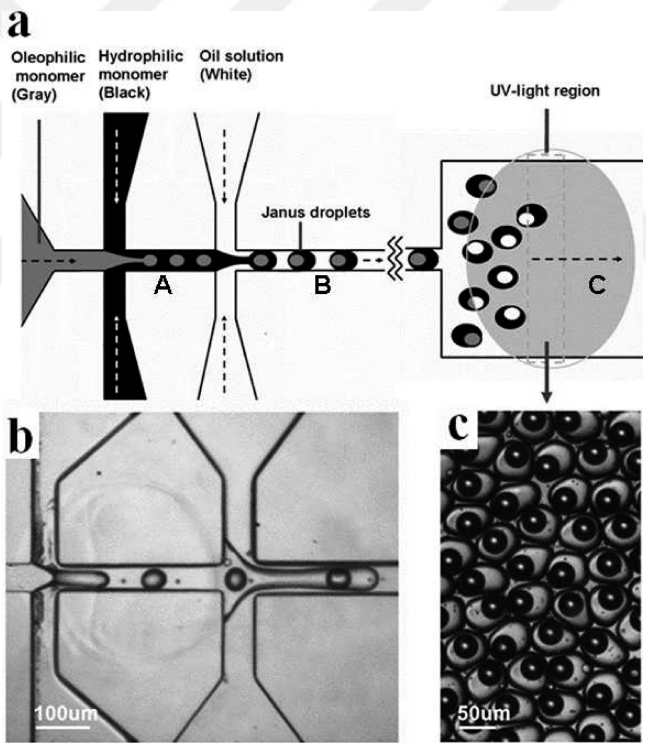

Figure 1.3: Schematic of the double emulsion method that has been utilized in literature for the synthesis of Janus particles. Note: Reprinted with permission from Chen CH, Shah RK, Abate AR, *et al.* Janus particles templated from double emulsion droplets generated using microfluidics. Langmuir. 2009;25(8):4320–4323. Copyright (2009) American Chemical Society. [65].

1.3 Double Emulsion

Double emulsion is a technique used in droplet-based microfluidics to generate encapsulated droplets inside a microfluidic device. The microchannels are selectively treated to create hydrophobic and hydrophilic segments and two or more droplet generation units allow for oil-water-oil or water-oil-water encapsulated droplets to be produced. Chen *et al.* [65,66] synthesized magnetically anisotropic Janus particles using an oil-water-oil double emulsion generator. The double emulsion was created by two in line droplet generators. As the encapsulated droplet proceeded in the main channel the density difference between the two droplets caused the inner droplet to be pushed towards the back of the encapsulating droplet. In this case the inner droplet contained magnetic nanoparticles and since it was moved to the back the entire droplet became anisotropic and therefore the particle that was created *via* polymerization was anisotropic as well. The schematic of their synthesis technique is shown in Figure 1.3. In order to provide support during UV polymerization, Thiele *et al.* [67] further improved this method to include a third consecutive droplet generator due to which the second inner droplet acted as a scaffolding. With this method particles having a hydrophilic/hydrophobic lobe and an outer hydrophilic shell were synthesized for potential use as surfactants for emulsion stabilization.

As discussed earlier the double emulsion method relies heavily on oil-in-water emulsions and this is why the synthesized particles are unable to encapsulate biomolecules. Consequently a lot of research is focused on utilizing multiple all-aqueous emulsions to synthesize Janus particles using this method [68].

1.4 Motivation

Even though microfluidic-based techniques provide a superior pathway for synthesizing Janus particles, the techniques available in literature are faced with fundamental limitations. Co-flow technique relies heavily on the diffusion length

scale to avoid mixing and for the maintenance of a clear interface between the two parallel flowing phases. In order to aavoid mixing the viscosities and velocities of the parallel flowing fluids need to be identical which is not possible in Janus particle synthesis since the two adjacent parts are inherently different.

Secondly, in case of the phase separation method, the constantly changing volume of the droplet due to solvent evaporation does not allow the system to achieve thermal equilibrium, and therefore predicting the shape of the synthesized particles is difficult [55]. Furthermore majority of the phase separation techniques utilize off-chip crosslinking which not only is a great inconvenience, but also leads to potential merging of droplets while being stored in off-chip containers.

In case of double emulsion method, the series of two or three consecutive droplet generation junctions presents a challenge to fine tune the flow rate combinations to generate encapsulated droplets continuously. Apart from that the density difference between the two droplets causes the inner droplet to be pushed towards the back of the encapsulating droplet but this only happens during the flow of the droplet in the continuous phase fluid while majority of the techniques utilize off-chip curing. Due to this the resulting particles might exhibit limited to no anisotropy.

The aim of this research is to design a microfluidic device for the simple and efficient synthesis of magnetically anisotropic Janus particles while avoiding the drawbacks of the already available methods namely; poor size distribution, off-chip processing and intermixing between the two Janus parts.

1.5 Overview of the thesis

The following paragraphs describe the layout of this thesis by outlining the contents of each chapter.

Chapter 2 discusses the design considerations and the possible geometries for the device. It starts off with introducing the flow focusing geometry and how the droplet generation takes place in that case. Then, the details of the numerical studies performed to optimize the droplet generation junction design are discussed and the comparison of the simulation data with the experimental data is presented to emphasize the reliability of the simulation data. Furthermore the design of the downstream channel is also discussed and a comparison between the serpentine geometry and a simple wider geometry is presented to emphasize the need of a stable droplet sequence during the polymerization step. Finally the chapter discusses the working fluids in the experimental setup which are the continuous phase and the dispersed phase. The recipes of the continuous phase and the dispersed phase fluids were optimized to generate continuous monodispersed prepolymer phase droplets. The recipe of the magnetic nanoparticles was also tailored to prevent agglomeration. Further the chapter describes a new technique where Janus particles can be synthesized by bringing together two different droplets and polymerizing them inside a microfluidic device. A number of geometries were experimentally tested to provide efficient merging of droplets from two sources in a microfluidic device. Among the geometries tested were asymmetric rectangular groove, circular merging section, tapered merging section and asymmetric cross-junction. The asymmetric cross-junction device exhibited highly efficient merging capability compared to the other geometries. Furthermore the orientation of the Janus droplets at the instance of merging determined if the contents of the droplets mixed homogeneously or if they stayed in a Janus orientation.

Chapter 3 presents the procedure adopted to produce monodisperse prepolymer phase droplets having unifromly spread magnetic nanoparticles. The recipe

of the dispersed phase was optimized by reducing the quantity of the highly viscous PEGDA 700 and increasing the quantity of the less viscous PEGDA 575. By doing this the nanoparticles were given a less viscous medium to spread in and therefore avoid agglomeration. Moreover the most suitable flowrate combination of the continuous and the dispersed phase was experimentally determined. Furthermore, by utilizing the magnetization data of the nanoparticles and a magnetic flux density map of the permanent magnet to be used in the experiments, the optimum magnetic flux density for the compartmentalization of the magnetic nanoparticles was determined and experimentally confirmed.

Chapter 4 discusses the imaging and the behavior of the Janus particles after the synthesis. It starts off with details of the synthesis procedure and proceeds with describing the scanning electron microscope imaging and how the imaging was improved by ensuring complete polymerization and complete removal of oil. It also contains the description of how the synthesis was affected by the concentration of the ferrofluid. Moreover it contains the optical microscope images, size distribution data and sem images of the synthesized Janus particles. It further elaborates on the motion of the Janus particles under the influence of an external magnetic field. Further in the chapter the results from the asymmetric cross-junction device that was utilized to synthesize Janus particles with one hemisphere containing iron oxide nanoparticles and the other containing either titanium dioxide or silicon dioxide nanoparticles are reported. The optical microscope images, scanning electron microscope image and the magnetic motion experiment observations have been included in this chapter.

Chapter 2

Device Design

The main components of a microfluidic device for the synthesis of Janus particles are: a droplet generator, a cross-linking section and an outlet for particle collection. In the following subsections the details of the device have been discussed and the pathway for the optimization of the device geometry has been provided.

2.1 Device for the synthesis of magnetic Janus particles

In droplet-based microfluidic devices there are three primary techniques to generate droplets continuously. The first is T-junction in which the continuous phase and dispersed phase channels are perpendicular to each other. The second one is co-flow junction in which the two fluids flow parallel to each other. The third one is flow-focusing in which the dispersed phase channel is enclosed between the two perpendicular continuous phase channels. These three geometries are shown in Figure 2.1.

Due to the presence of chemicals such as Polyethylene glycol diacrylate (PEGDA), photoinitiator compound 2-Hydroxy-2-methylpropiophenone (HMP)

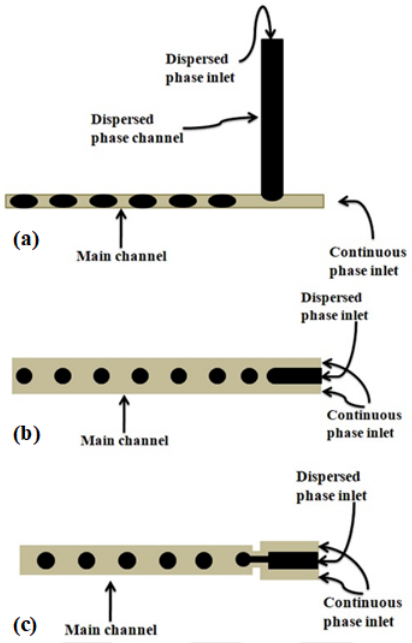

Figure 2.1: (a) Droplet generation junction schematic for a T-junction geometry. (b) Droplet generation junction schematic for a co-flow geometry. (c) Droplet generation junction schematic for a flow-focusing geometry [69].

and magnetic nanoparticles in the dispersed phase fluid, the droplet generator was designed as a flow-focusing geometry. The reason for this is that these chemicals have the tendency to stick to the PDMS walls, and T-junction geometry design gives the dispersed phase the opportunity to stick to the main channel wall while generating droplets. On the other hand, a flow-focusing droplet generator creates a complete encapsulation of the dispersed phase inside the continuous phase stream and does not let the dispersed phase stream touch the channel walls.

The droplet generation junction is at the intersection of three microchannels; two of them facing each other towards the junction for the oil flow, and the third one perpendicular to and in between the two side channels for the dispersed phase fluid as shown in Figures 2.2 and 2.3. These figures show two initial designs that were developed to test the polymerization of prepolymer phase droplets inside the microfluidic device. The entrance of the dispersed phase channel into the main channel is transitioned *via* an orifice. The orifice ensures droplet formation just as the dispersed phase stream exits the junction instead of droplet formation

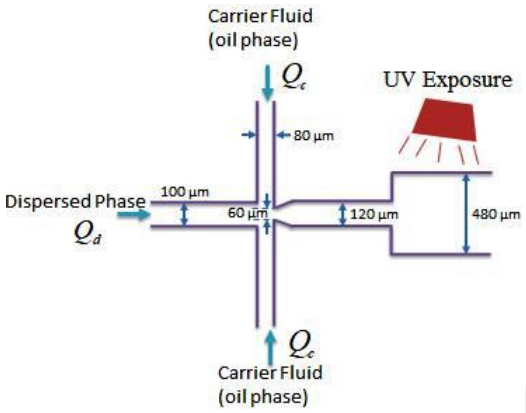

Figure 2.2: The schematic of the device that utilizes a flow-focussing geometry to generate droplets and a wider geometry downstream to transport the droplets to the outlet while they are being polymerized.

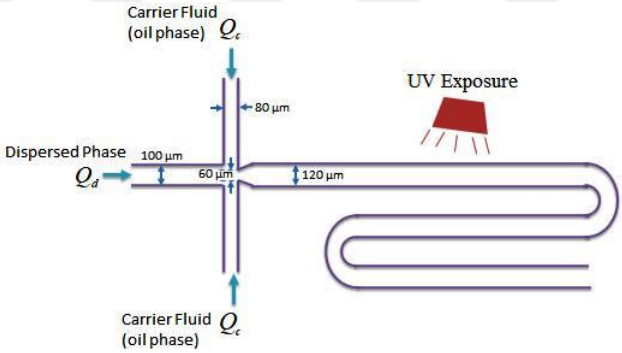

Figure 2.3: The schematic of the device that utilizes a flow-focussing geometry to generate droplets and a serpentine geometry downstream to transport the droplets to the outlet while they are being polymerized.

downstream. Moreover the presence of an orifice gives improved control over the size of the generated droplets [70].

2.1.1 Numerical studies

The droplet generation junction was a flow-focusing geometry shown in Figure 2.5. The Reynolds number Re was calculated as 9.12×10^{-3} using equation 2.3. The density of the continuous phase fluid is 857.5 kg/m^3, the velocity of the continuous phase fluid is 2.775 mm/s and the characteristic length is 120μm. The viscosity

of the dispersed phase stream is calculated as 0.0313 Ns/m^2 using the gambill method [71]. Reynolds number Re less than 2000 generally indicates that the flow is laminar. Laminar flow is characterized by uniform, organized fluid motion with well-defined streamlines. For Reynolds number Re less than 1, $Re \ll 1$, the flow is considered to be in the creeping flow regime [72]. Creeping flow is a particular type of laminar flow which takes place at low speeds or extremely small characteristic lengths. In the creeping flow regime, viscous forces are dominant and inertial forces are negligible. Moreover the flow patterns are highly ordered and repetitive. In the creeping flow regime, the motion can be described by the Stokes equations. Stokes equations are attained by disregarding the inertial terms in the Navier-Stokes equations as shown in equation 2.2.

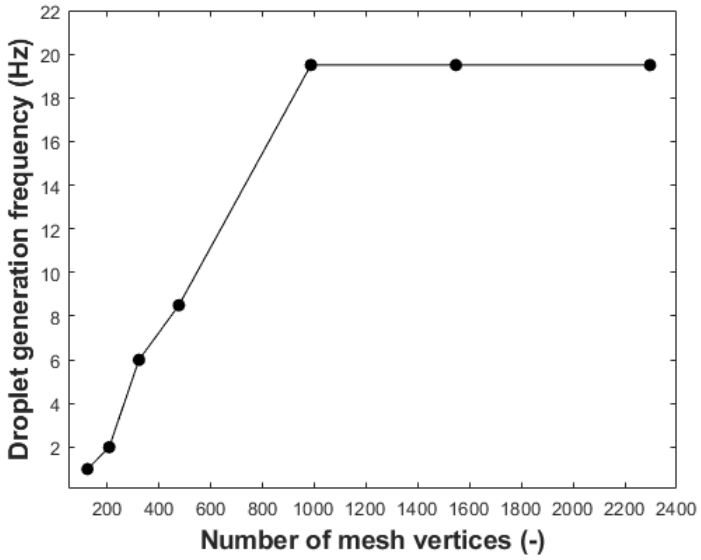

Figure 2.4: Mesh independence of the numerical studies.

The level set method utilizes equations 2.4 and 2.5 to evaluate the density and viscosity of the two-phase medium. Here; Φ represents the level set variable for the fluids with discrete values between 0 and 1. In order to ascertain the optimum mesh size for the numerical studies, the simulations were performed at seven different mesh settings extremely coarse, extra coarse, coarser, coarse, normal, fine and finer. For simulating a droplet generation process like this one there is a balance between the computational time and accuracy of the solution. The finer the mesh size, the more accurate the solution but if the solution converges

to the same value for a number of mesh sizes then it is preferable to select the coarser mesh size in order to save simulation time. For this reason simulations were performed for a Q_c value of 4.0 μL/min and a Q_d value of 0.2 μL/min for the seven mesh sizes. The mesh independence plot of the numerical studies is shown in Figure 2.4. As it can be seen in the Figure, the droplet generation frequency is inaccurate and low at coarser mesh sizes, but as the mesh size becomes finer (and the number of mesh elements increases) the frequency value becomes higher and finally converges at a value of 19.5 Hz. After this value the frequency does not increases further even at a finer mesh size which means that the number of mesh vertices 987, which corresponds to the mesh size normal, is an accurate representation of this simulation and a finer mesh is not required to make it more accurate. Therefore the mesh size was selected as normal for all the numerical studies in order to reduce the computational time while keeping the results accurate.

$$\rho(\frac{\partial v}{\partial t} + \mathbf{v} \cdot \nabla \mathbf{v}) = -\nabla p + \mu \nabla^2 \mathbf{v} + \mathbf{f} \tag{2.1}$$

$$\nabla p = \mu \nabla^2 \mathbf{v} + \mathbf{f} \tag{2.2}$$

$$Re = \frac{\rho U L}{\mu} \tag{2.3}$$

$$\rho = \rho_1(1 - \Phi) + \rho_2 \Phi \tag{2.4}$$

$$\mu = \mu_1(1 - \Phi) + \mu_2 \Phi \tag{2.5}$$

2.1.1.1 Optimum Angle of Inclination of Continuous Phase Channels

In a flow-focusing device the angle of inclination of the continuous phase channels is an important parameter (shown in Figure 2.6) since it facilitates the focusing of the dispersed phase. Initially the angle θ was kept zero which means that the continuous phase channels were horizontal but during several experiments it was observed that the nanoparticles accumulate at the junction and clog the passage as shown in Figure 2.7. In order to eliminate the channel clogging problem, the angle θ was increased. In order to find the optimum angle of inclination, numerical simulations were conducted for two θ values: 30° and 60°. The numerical simulations were performed using olive oil as the continuous phase and deionized water as the dispersed phase. The simulations were performed for a range of flow rates of the continuous phase Q_c, and the dispersed phase Q_d. In the first set the value of Q_d was fixed at 1.0 μL/min and Q_c was varied from 2.0 μL/min to 5.0 μL/min. In the second set of experiments the value of Q_c was fixed at 3.0 μL/min and Q_c was varied from 0.225 μL/min to 1.0 μL/min The ratio Q_d/Q_c is known as the flow rate fraction ϕ and it is useful for quantifying the flow rate in cases where one flow rate is kept constant and the other one is varied.

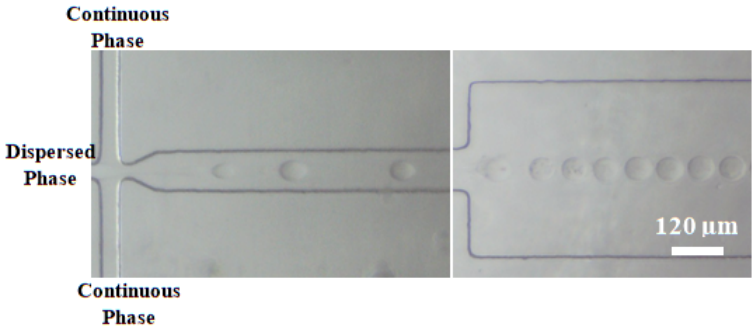

Figure 2.5: Optical microscope image showing the microfluidic device with a wider channel downstream.

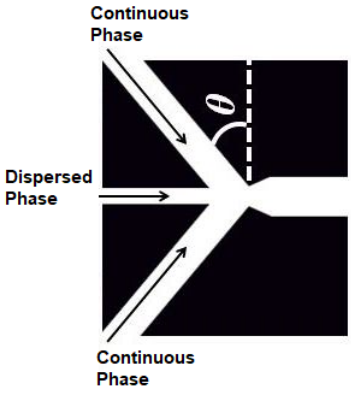

Figure 2.6: Droplet generation junction schematic showing the dispersed phase inclination angle θ

Figure 2.7: Optical microscope image showing the clogging of the junction due to accumulation of nanoparticles.

2.1.1.2 Droplet size

In order to compare experimental results to the simulations, droplet size was measured for one set of simulation data and compared to the experimental data. Figure 2.8 (a) shows the comparison of the experimental droplet size with the one obtained from the simulations. It can be observed that the data is in good agreement with an error of around 4.0%. This error is calculated by using the standard error formula. The error bars are evaluated by measuring the size of five consecutive droplets and finding their average and their standard deviation.

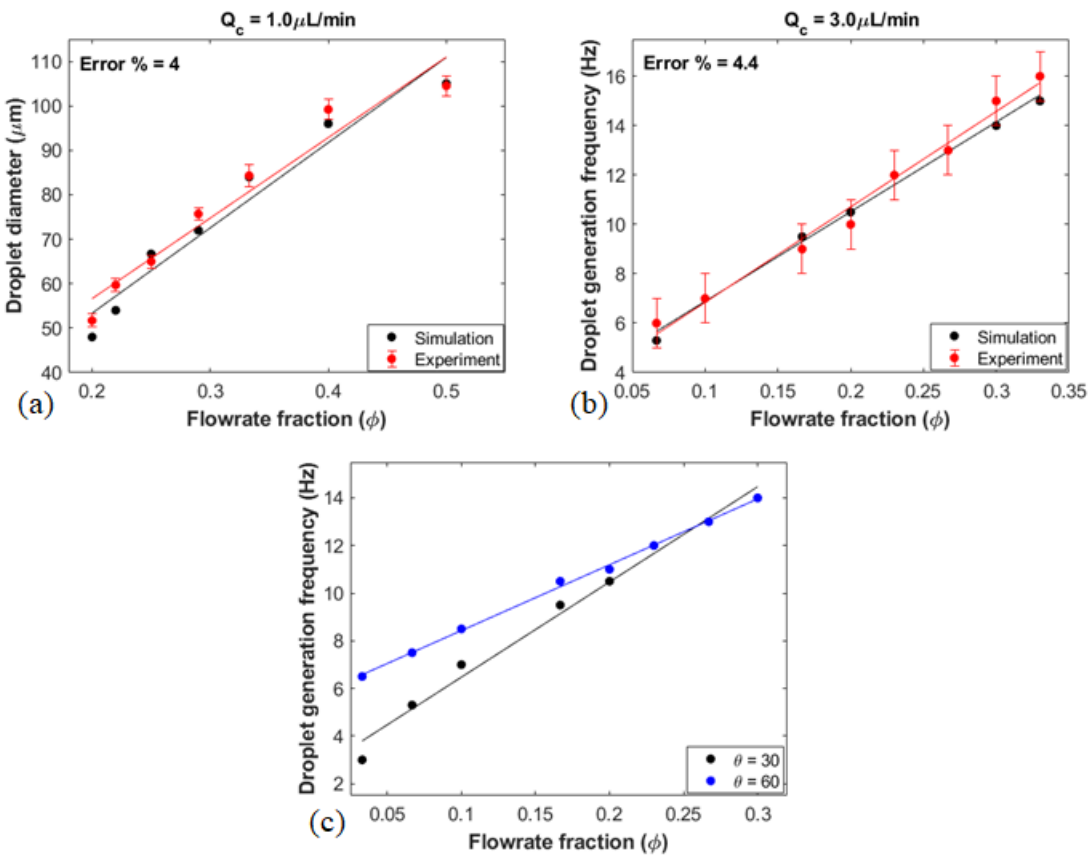

Figure 2.8: (a) Droplet size comparison between numerical simulation data and experiments with $\theta = 60°$. (b) Droplet generation frequency comparison between numerical simulation data and experiments with $\theta = 60°$. (c) Droplet generation frequency comparison between $\theta = 30°$ and $\theta = 60°$. The droplet generation frequency of the device with $\theta = 60°$ is greater than that in case of $\theta = 30°$.

2.1.1.3 Droplet generation frequency

In the same manner droplet generation frequency was calculated for one set of simulation data and compared to the experimental data. Figure 2.8 (b) shows the comparison of the experimental droplet generation frequency with the one obtained from the simulations. In this case as well the data obtained from numerical simulations shows good conformity with the experimental data. The error bars are evaluated by finding the number of droplets generated in one second for two consecutive seconds and calculating their difference.

Both the values of θ resulted in stable droplet generation over a range of flow rate ratios. The droplet generation frequency comparison between the two devices is shown in Figure 2.8 (c). The graph shows that the droplet generation frequency is generally higher in case of $\theta = 60°$ as compared to $\theta = 30°$ in the range $0 < \phi < 0.25$. This shows that the device with $\theta = 60°$ is most efficient in droplet generation in this range of ϕ.

The next step for the generation of the particles is to cross-link the generated droplets. For that purpose two potential geometries were proposed to increase the residence time of the droplets from the droplet generation junction to the outlet of the device, thus giving enough time for the ultraviolet cross-linking to complete.

2.1.2 Microreactor with serpentine channel

Serpentine geometry has been used in earlier works in order to increase the residence time of droplets inside a microfluidic device. Due to the frequent U-shaped turns a longer length of microchannel can be adjusted in the same area of the device. The velocity of the droplets and the required residence time can be used to calculate the total length of the serpentine channel. In this device a droplet train was obtained as shown in the Figure 2.9. Since the droplet generation velocity is the same as the droplet transportation velocity this device was prone to be affected by small inconsistencies in the flow rate of the liquids which caused the droplet train sequence to be disturbed and in turn caused non-uniform size and shape of the polymer particles.

2.1.3 Microreactor with wider channel

Increasing the width of a microchannel results in the reduction of velocity of the flowing droplets in case of a constant volumteric flow rate at the inlet. For this reason a wider channel downstream of the droplet generation junction was

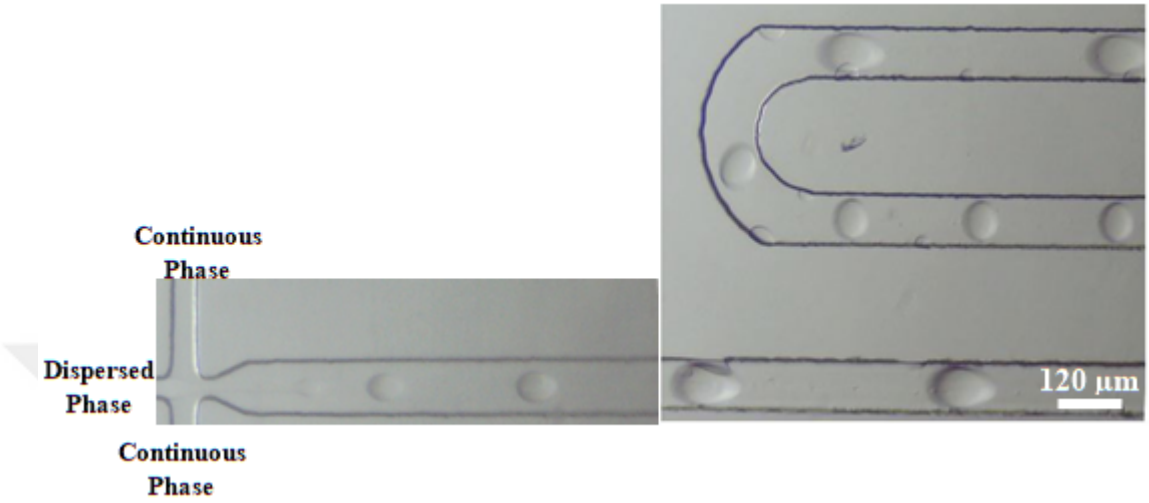

Figure 2.9: Optical microscope image showing the microfluidic device with a serpentine channel downstream.

proposed as a potential geometry for the cross-linking section. Unlike serpentine geometry, where the droplets are not supposed to come into contact at all, a wider channel downstream significantly slows down the velocity of the droplets and therefore causes them to merge. In order to avoid the merging of adjacent droplets it is necessary in this case to add a surfactant to the continuous phase fluid. A surfactant is a fluid that creates a chemical barrier between two interfaces that stabilizes them and prevents transport of any fluid through that barrier. Thus droplets flowing in a carrier fluid containing a surfactant will not merge even if they physically come into contact.

From the above discussion it was concluded that the device with $\theta = 60^{\circ}$ would be the most efficient to use for further experiments as shown in Figure 2.10.

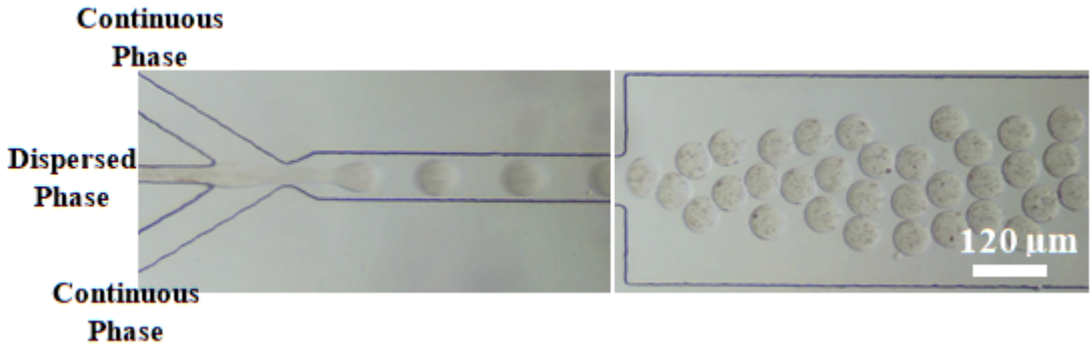

Figure 2.10: The optical microscope image of the droplet generation inside the device with the modified angle $\theta = 60°$.

2.2 Synthesis of Fe_2O_3/SiO_2 and Fe_2O_3/TiO_2 Janus particles

Janus particles with magnetic anisotropy could be useful for many applications, and adding another anisotropy to the particle would allow the particles to be employed for specialized applications. Therefore, the research idea was extended towards attaining Janus particles with dual properties provided by two different types of nanoparticles. For this purpose, the most important step was to bring together the two types of nanoparticles in a controlled manner. The schematic of the device used for this synthesis is shown in Figure 2.11 (a) and the optical microscope image of the device is shown in Figure 2.11 (b).

In droplet-based devices, droplets are used as micro-reactors therefore the aim is to merge two droplets having different types of nanoparticles in the device. For this purpose four potential droplet merging geometries were designed, fabricated and tested and the device with the best performance was chosen for the experiments.

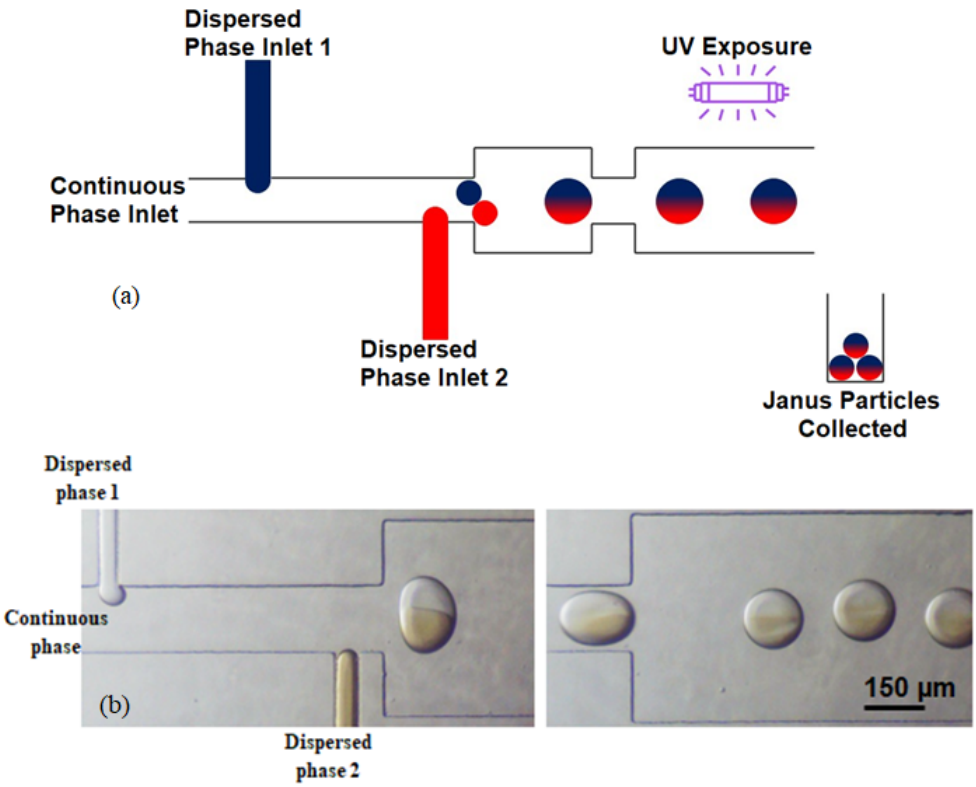

Figure 2.11: (a) Schematic of the microfluidic system for Fe_2O_3/SiO_2 and Fe_2O_3/TiO_2 Janus particle synthesis. (b) Optical microscope image showing the microfluidic device for Fe_2O_3/SiO_2 and Fe_2O_3/TiO_2 Janus particle synthesis.

2.2.1 Alternating droplet generation

In order to extend the current research to other functionalities, initial experiments were performed to obtain alternating droplets of monomer solution containing two different types of nanoparticles (namely iron oxide and silicon dioxide). In this context, five geometries were considered for the generation and merging of the droplets. In the next subsections devices having alternating droplet generator, shown in Figure 2.12, coupled with a merging geometry have been discussed. The device consists of a central continuous phase channel and two side channels for two different types of dispersed phases [73,74]. The value of the angle α was 2.5°.

In the initial experiments the monomer solutions were used directly after mixing nanoparticles in them. Figure 2.13 (a) shows how in this case the two streams merge together instead of forming alternating droplets (bottom stream contains

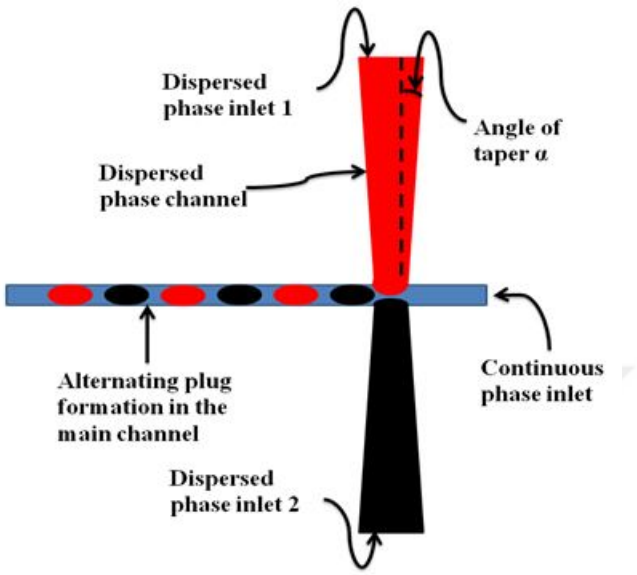

Figure 2.12: Schematic of the alternating droplet generation device [73].

silica nanoparticles and the top stream contains iron oxide magnetic nanoparticles). The reason for this is that the monomer solution has an extremely high viscosity (140cP) due to which both streams enter the main channel at the same time. In order to tackle this problem, the monomer solution was diluted with water (since the monomer is water soluble). It was observed that with 50% water dilution the alternating pattern was achieved as shown in Figure 2.13 (b). As the water dilution was increased further it reduced the polymerization ability of the monomer and as the dilution was decreased the alternating pattern was not observed.

In the next subsections devices having alternating droplet generator [73], shown in Figure 2.12, coupled with a merging geometry have been discussed.

2.2.1.1 Asymmetric merging section

In this device the alternating droplet generator was followed by an asymmetric rectangular groove that was designed to slow down droplets and induce their coalescence [75]. The droplet merging sequence is shown in Figure 2.14. It can be seen in the sequence that the rectangular section caused the red and blue

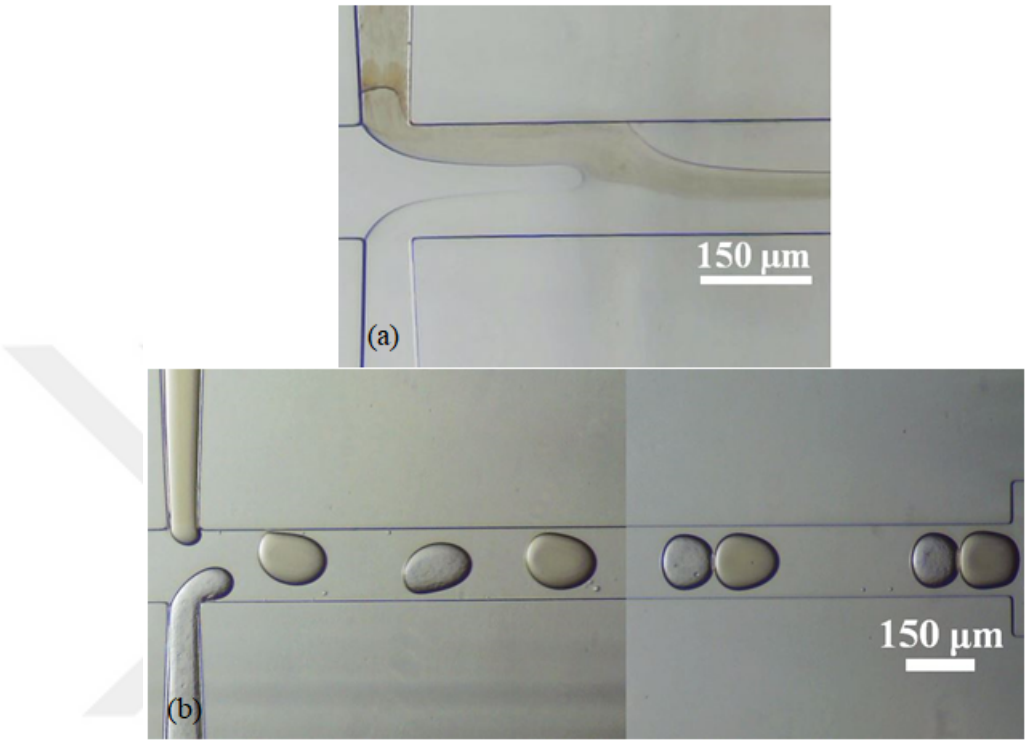

Figure 2.13: (a) An example of undesired merging of streams due to high viscosity of both dispersed phases. (b) An example of perfect alternating droplet generation and droplet transport downstream.

droplets to slow down and come into close proximity. As they came in contact with each other the oil film between the two droplets kept draining away and finally the droplets coalesced and kept moving further downstream. It must be noted here that the droplets merged after a rotation from a head-on to a sideways position in this geometry.

2.2.1.2 Circular merging section

The circular merging section was another method of slowing the droplets and letting them come in contact with each other until the oil film drains away [76]. The sequence in Figure 2.15 shows how the droplets closed in on each other and finally merged. The merging in this case was head-on as compared to sideways after rotation in asymmetric geometry. The advantage of having a head-on merging

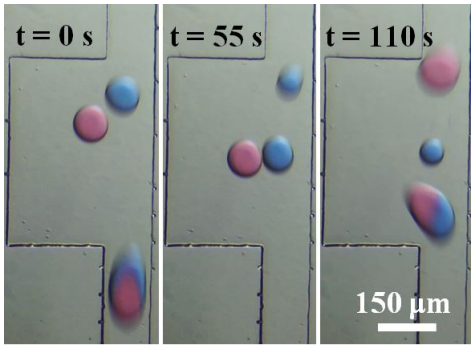

Figure 2.14: Droplet merging sequence in the asymmetric merging channel

is that there is lower time-lapse between droplets coming closer and merging.

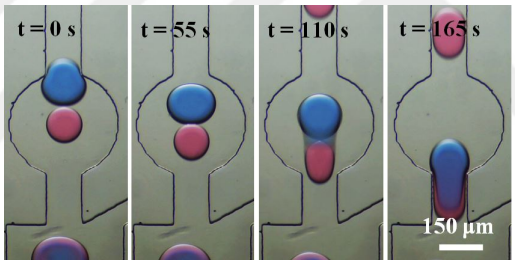

Figure 2.15: Droplet merging sequence in the circular merging channel

2.2.1.3 Tapered merging section

This design was yet another method of slowing droplets and inducing coalescence [77]. But unlike the previous two designs this one did not have specific center of merging. As shown in Figure 2.16 the droplets were slowed down as they move across the tapered section but since there is enough space for the droplets to spread out they do not come into close proximity with each other and therefore merging is less efficient than in previous designs.

2.2.1.4 Pillar-based merging section

Another potential merging geometry was the pillar induced merging method [78]. In this method the droplets were forced through a series of converging pillars

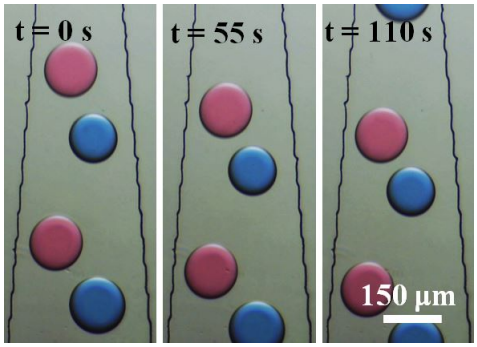

Figure 2.16: Droplet merging sequence in the tapered merging channel

and as a result droplets slowed down and came into close proximity as shown in Figure 2.17.

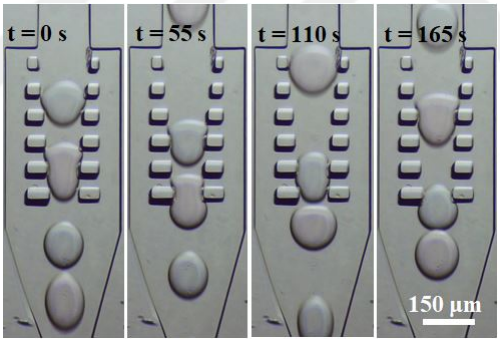

Figure 2.17: Droplet merging sequence in the pillar-based merging channel

Although the droplets were forced to come into proximity this geometry creates fabrication problems due to the feature size being as low as 20 x 20 microns. Some examples of the fabrication inconsistencies are shown in Figure 2.18. Due to the pillar being a high aspect ratio feature it often got removed from the microchip.

2.2.1.5 Co-flowing merging device

The idea behind this merging technique was that by changing the width of the main channel the two droplet phases could be made to generate merged droplets at the junction without any need for a merging geometry downstream [3]. The width of the channel (w) was reduced from 150 microns to 100 microns. Due to this change in the width the two droplet streams generated merged droplets at

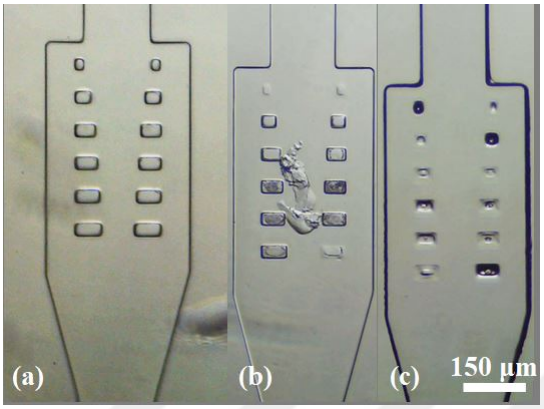

Figure 2.18: Fabrication defect in the pillar-based merging channel

the junction as shown in Figure 2.19.

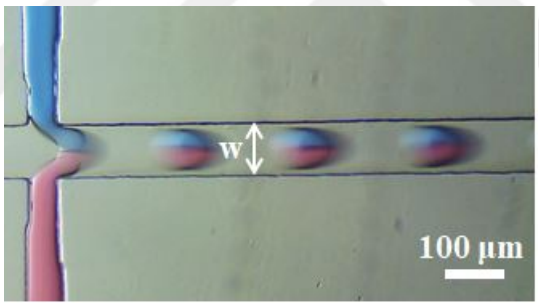

Figure 2.19: Droplet merging sequence in the tapered merging channel

The methods that were designed and tried up until this point were all dependent on the cross-junction geometry shown in Figure 2.12. Although this method can generate synchronized droplets efficiently, there were instances where the droplet diameter and droplet spacing were not uniform which greatly hinders the merging process. In order to tackle this issue the cross-junction was made asymmetric to facilitate continuous droplet generation and merging. This is discussed in detail in the next section.

2.2.1.6 Asymmetric cross-junction merging device

As discussed previously a typical cross-junction device has the drawback of droplet spacing not being uniform due to which droplets did not catch up to

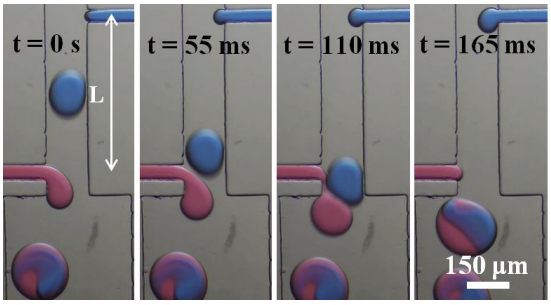

Figure 2.20: Droplet merging sequence in the asymmetric cross-junction merging device

each other and thus were unable to merge. In order to resolve this, the two dispersed phase channels were designed to be at a distance of $L = 560$ *microns* so that as the droplet of the first dispersed phase is generated it catches up with the droplet of the second phase while it is generating the droplet. This process is shown in Figure 2.20. A wider segment is also added just after the second dispersed phase channel to facilitate droplet merging [79–81].

Although the device exhibited great merging efficiency it was important to ensure that the Janus orientation of the droplets was maintained during and after the merging process. For this reason the orientation of droplet interaction during the merging process was observed. Figures 2.21 (a) and 2.21 (b)show how the angle of droplet interaction affects the mixing procedure in the droplets. In Figure 2.21 (b) the angle of interaction is low and therefore the droplets merge in an almost sideways orientation resulting in a Janus configuration. This Janus configuration is further maintained by the chaotic advection mixing inside the droplet due to the two phase flow which is brought about by the presence of the immiscible interface between the continuous phase and the dispersed phase. The velocity profile of a droplet flowing inside an immiscible fluid is different from a single phase flow velocity profile. The droplet experiences recirculation zones due to this modified flow profile. The recirculation zones inside the droplet are symmetric if the flow conditions are symmetric with reference to the centre of the droplet as show in Figure 2.21 (a). These symmetric recirculation zones ensure that the two constituents of the droplet, which are separated along the centre of the droplet, do not merge.

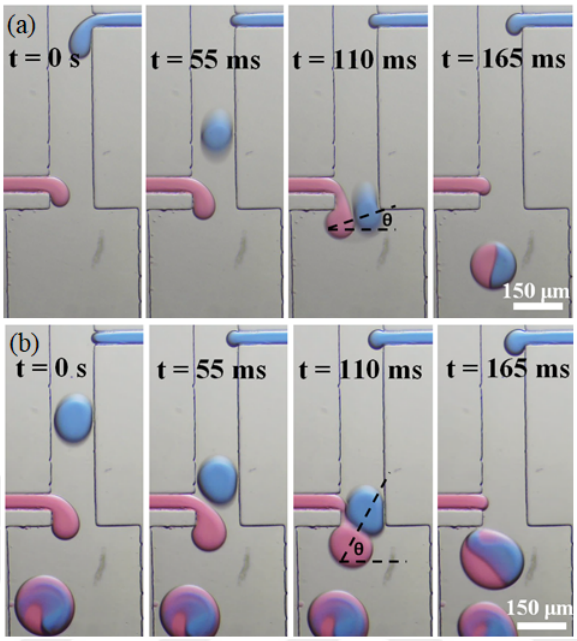

Figure 2.21: (a) A low angle of interaction results in a symmetric distribution of the two constituents. (b) A high angle of interaction results in a chaotic mixing of the constituents.

On the other hand if the angle of interaction is high as shown in Figure 2.21 (b), the droplets merge in an almost head on orientation and the constituents mix in a chaotic manner till the contents of the droplet become homogenous. This chaotic mixing is also assisted by the recirculation zones but since the contents of the droplet were not symmetrically separated at the beginning, they are mixed homogenously unlike the first case.

The angle of interaction is governed by the ratio ($\phi = Q_d/Q_c$) of the volumetric flow rates of the dispersed phase (Q_d) and the continuous phase (Q_c) fluids. If the value of ϕ is low, the droplet size is smaller therefore giving the second droplet to completely exit the channel without interacting with the first droplet and finally the two droplets interact just at the edge of the main channel as shown in Figure 2.21 (a). In contrast when the value of ϕ is high the droplet size is bigger and the second droplet is blocked by the first droplet and the second droplet is unable to exit the main channel. As a result the two droplets interact almost head-on at a high interaction angle as shown in Figure 2.21 (b).

2.3 Working Fluids

2.3.1 Carrier Fluid

Initially a mixture of olive oil and hexane was used as the continuous phase fluid. The reason for using a mixture is that olive oil has a viscosity of around 56.2 cP [82] which is much similar to the viscosity of the monomer PEGDA ($\simeq$ 70 cP as per the manufacturer's website). Due to this the droplet generation process cannot be clearly observed(as shown in Figure 2.22a) and there is possibility of the dispersed phase fluid sticking to the channel walls. In contrast to this, the mixture of olive oil and hexane has a much lower viscosity and the droplet generation process can be clearly observed as shown in Figure 2.22b.

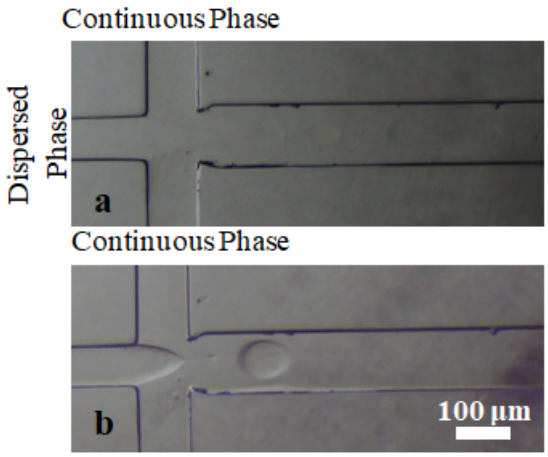

Figure 2.22: Optical microscope image in case of a) olive oil as the continuous phase; the droplet generation process cannot be clearly observed. b) olive oil plus hexane as the continuous phase; the droplet generation process can be clearly observed.

Olive oil acts as the viscous fluid, applying pressure at the junction to cause droplet generation and also provides a thin film between the droplets and the channel walls. Hexane is a hydrocarbon and has a small wetting angle with PDMS and mixes easily with the oil phase. Due to these properties, hexane is mixed with olive oil to act as the continuous/carrier phase. In addition to this, as has already been mentioned, surfactant Span 80 is used in order to avoid droplet

merging. In the absence of a surfactant, two adjacent droplets keep coming closer and the thin fluid film of continuous phase fluid keeps getting narrower until the two droplets merge as shown in Figure 2.23. In contrast to this, the presence of a surfactant creates the Marangoni Effect [83] which counteracts the thinning of the fluid film and prevents the merging of droplets as shown in Figure 2.24.

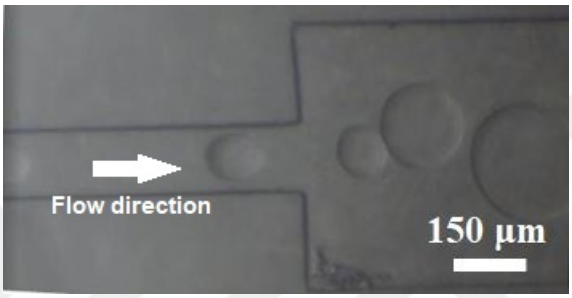

Figure 2.23: Optical Microscope image showing droplet merging at the entrance of the wider channel because of absence of any surfactant.

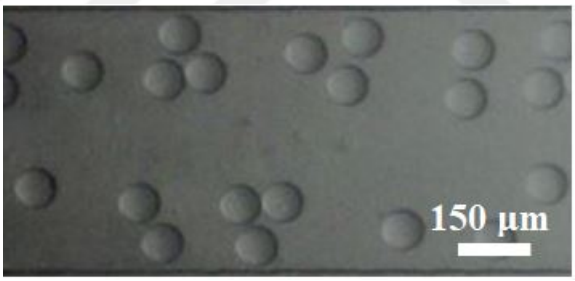

Figure 2.24: Optical Microscope image showing droplets being transported without any merging due to the presence of surfactant Span 80.

The main challenge faced in this experimental procedure was the accumulation of surfactant at the channel walls as shown in Figure 2.25. The reason for the surfactant accumulation was the presence of hexane in the continuous phase; since hexane is volatile it vaporizes during the experiment causing the surfactant, which was dissolved in hexane, to be deposited on the microchannel walls.

In order to tackle this issue, hexadecane was added to the olive oil and hexane mixture since hexadecane is not as volatile as hexane but has the same effect as hexane (since both are hydrocarbons). A mixture of olive oil 64% (v/v), hexadecane 30% (v/v) and hexane 6% (v/v) is used as the continuous phase

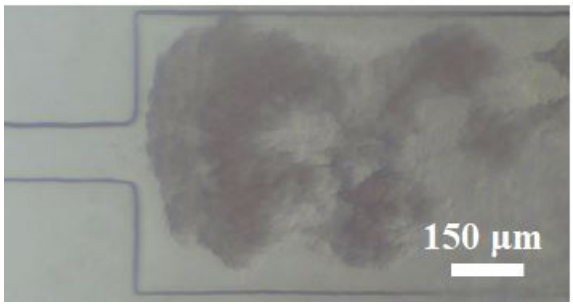

Figure 2.25: Optical microscope image showing surfactant accumulation at the microchannel walls.

with 2wt% Span80 surfactant which is added to avoid droplet merging in the downstream channel.

2.3.2 Dispersed Phase Fluid

The dispersed phase fluid has a number of constituent parts. For the current work, Poly(ethylene glycol) diacrylate (PEGDA) is used as the monomer phase. It is a derivative of polyethylene glycol and is suitable for use in a number of drug delivery and tissue engineering applications. The photoinitiator compound is 2-Hydroxy-2-methylpropiophenone. As the photo-initiator is mixed with the monomer in a specific ratio, exposure to UV radiation causes polymerization (solidification). PEGDA 575 80.6% (v/v), photo initiator HMP 13% (v/v), Tween 20 3.2% (v/v) and ferrofluid containing 0.25g/mL SPIONs suspended in deionized water 3.2% (v/v) are mixed to serve as the dispersed phase.

The synthesis of magnetic nanoparticles for this work was conducted by using iron chloride salts and ammonia solution. During the course of the experiments different recipes were tried and it was observed that in order to obtain smaller particles, the use of a surfactant like sodium dodecyl sulfate (SDS) is helpful since it covers the surface of the particle and does not allow the growth beyond a point and it also keeps the nanoparticles (NPs) from adhering to each other which is really important in the current setup. It was observed that the nanoparticles settle down overnight and agglomerate since the particles are larger and have a

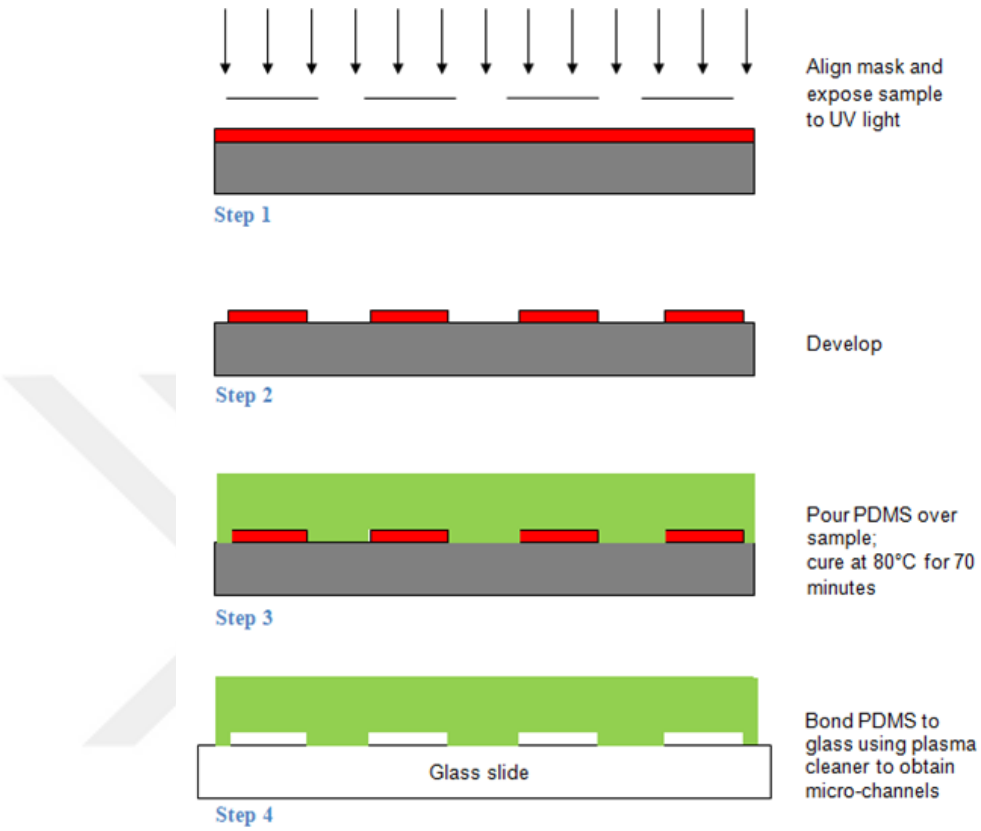

Figure 2.26: Schematic showing the fabrication steps of the microfluidic device [69].

tendency to agglomerate. Whereas the batch synthesized by incorporating SDS in the recipe does not show any agglomeration even after 48 hours.

2.4 Fabrication of the device

The fabrication of each microfluidic device was done using the conventional soft lithography technique as shown in Figure 2.26. The SU8 master mold was prepared on a polished 4" Si wafer in the clean room by using the Mask Aligner and Nanoimprint Lithography equipment. After making the SU8 master, the PDMS mold was prepared in the microfluidics laboratory and then it was bonded to a glass slide using an oxygen plasma cleaner.

Chapter 3

Experimentation

In our initial experiments we synthesized polymeric Janus particles with magnetic nanoparticles embedded in them as shown in the schematic in Figure 3.1. For the particle size and quality to be uniform the uniformity of droplet size and form was of utmost important. In the following sections the optimization of the flowrate combinations, recipe of the dispersed phase fluid and the magnetic flux density will be discussed.

The experimental setup consisted of an optical microscope, two syringe pumps, a microfluidic device and an ultraviolet source as shown in Figure 3.2. After the microchip fabrication (which has been described in Appendix A), the next step was to prime the device with the continuous phase. The capillary tubing was inserted in the continuous phase inlet and the continuous phase was injected using a syringe pump. The continuous phase was kept flowing through the microchannels for at least five minutes so as to ensure complete hydrophobicity of the channels. After that the dispersed phase capillary tubing was inserted in the dispersed phase inlet and the syringe pump for the dispersed phase was started and the droplet generation was observed using an optical microscope. When the droplet generation became stable, the UV lamp was turned on and the microparticles were collected in a clean centrifuge tube. The Ultraviolet radiation exposure setup consisted of a UV lamp and an aperture placed on top of the device in

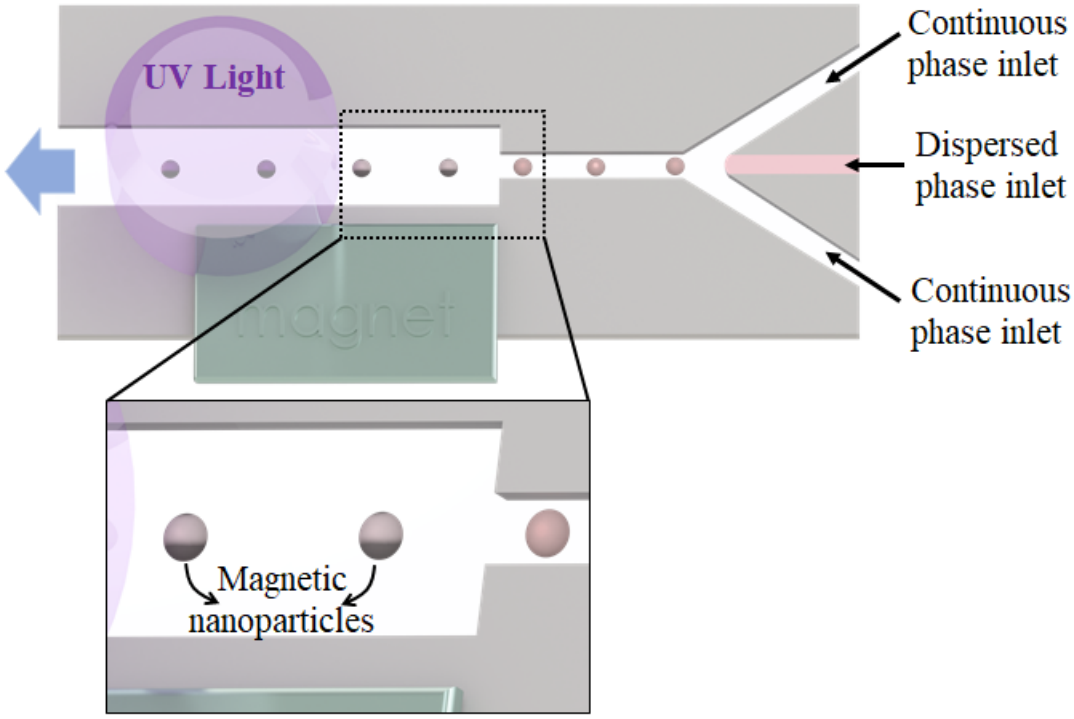

Figure 3.1: Schematic of the microfluidic system. Note: Reprinted with permission from Saqib, Muhammad, Batur Ercan, and E. Yegan Erdem. "Synthesis of Anisotropic Magnetic Polymeric Janus Particles by In Situ Separation of Magnetic Nanoparticles in a Microfluidic Device." Langmuir 39.48 (2023): 17080-17087. Copyright 2023 American Chemical Society [84].

order to expose only the specific parts of the device to UV radiation. After the particles were collected in a centrifuge tube, excess oil was removed from them and the particles were washed with pure ethanol (to remove oil) multiple times (atleast five times) and DI water (to remove uncured monomer) alternately at a centrifuge speed of 500rpm. The particles were transferred on top of a SEM stub covered with conducting tape using a micropipette. The sample was then coated with around 5nm of gold and then observed under the SEM. Initially the microfluidic device was utilized to synthesize polymer particles that do not contain magnetic nanoparticles. The purpose of this exercise was to test the ultraviolet polymerization setup.

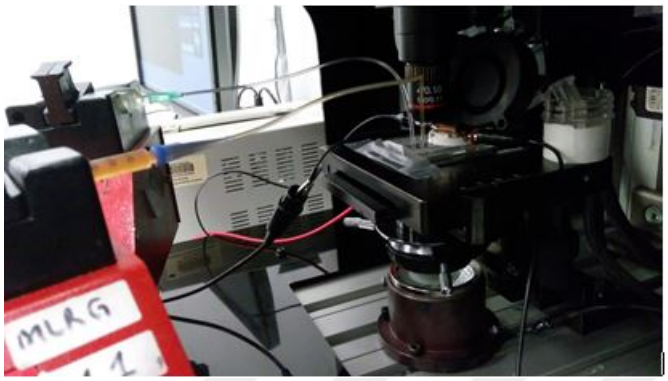

Figure 3.2: Experimental setup showing the microfluidic device, the syringe pumps and the optical microscope.

3.1 Generating Monomer Droplets

The effect of a magnetic field in the monomer solution was observed by mixing the monomer PEGDA (Poly ethylene glycol diacrylate) with the synthesized ferrofluid. The components (1mL PEGDA 575, 0.5 mL PEGDA 700, 60 μL Photo initiator Darocur 1173, 0.3 mL Ferrofluid (1 g/mL of NPs in DI water)) were poured in a 2 mL centrifuge tube one by one using a pipette and then the resultant solution was mixed thoroughly using a vortex mixer. This solution was used as the dispersed phase.

The dispersed phase and continuous phase were injected into the device using syringe pumps. Figure 3.3 shows the droplet generation in this case. It was observed that the concentration of magnetic NPs was not uniform in the droplets. The cause of this inconsistency is the non-uniform mixing of the magnetic NPs in the monomer solution. The non-uniform mixing caused the NPs to agglomerate in the dispersed phase. As more time passed, the NPs agglomerate even more in the dispersed phase tubing.

The issue of non-uniform mixing in the dispersed phase was crucial and in order to improve it 0.35 mL deionized water was added to the dispersed phase so as to facilitate the mixing of magnetic NPs. Even though this addition caused

Figure 3.3: Continuous generation of monomer droplets (containing accumulated magnetic nanoparticles) in the microfluidic device.

the nanoparticles to spread much more evenly in the droplets, it resulted in non-uniform droplet size as shown in Figure 3.4.

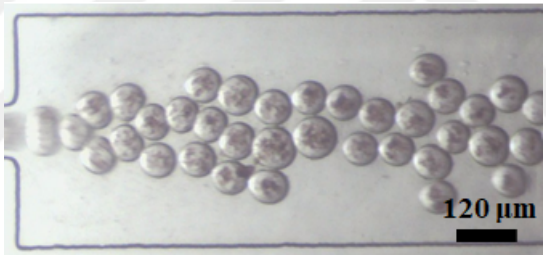

Figure 3.4: The droplet size is non-uniform due to non-uniform mixing of the ferrofluid in the dispersed phase.

From these observations it was concluded that with this recipe the magnetic NPs do not disperse uniformly in the monomer solution and due to this the droplet generation is non-uniform. In order to improve the droplet generation in case of monomer solution containing magnetic NPs the following key points were incorporated in our recipe for the dispersed phase.

Figure 3.5: Optical microscope image showing the magnetic nanoparticles spread uniformly in the droplets.

Figure 3.6: Optical microscope image showing the magnetic nanoparticles spread uniformly in the droplets.

- The percentage by volume of the more viscous PEGDA 700 needed to be lowered since the less viscous PEGDA 575 has a viscosity of around 70 cP (according to supplier's website), and the viscosity of PEGDA 700 is much higher (147 cP [85]) than that which hinders the dispersion of NPs in the liquid. Therefore it was proposed that eliminating the highly viscous PEGDA 700 would improve the distribution of NPs in the droplets.
- The concentration of the magnetic NPs needed to be optimized, because a very high concentration causes agglomeration and a very low value did not allow observation under an optical microscope.
- Use of a surfactant in the dispersed phase was essential because this would prevent agglomeration of NPs in the dispersed phase. In this context the use of Tween 20 was proposed.

The new recipe components (0.5 mL PEGDA 575, 80 μL Photo initiator Darocur 1173, 40 μL Ferrofluid (0.25g/mL of NPs in DI water) and 20 μL Tween 20) were poured in a 2 mL centrifuge tube one by one using a pipette and then the resultant solution was mixed thoroughly using a vortex mixer. This solution was used as the new dispersed phase.

It can be observed in Figure 3.5 that when the dispersed phase does not contain the highly viscous PEGDA 700, the droplet generation became uniform and the distribution of magnetic NPs in the droplets is also uniform. As the continuous phase flowrate was increased to 2.0 μL/min, the droplet size decreases but remains uniform and the NP distribution also remains uniform as shown in Figure 3.6.

By improving the quality of nanoparticles as mentioned, and by using a higher proportion of the less viscous PEGDA 575 as compared to PEGDA 700, the magnetic nanoparticles were made to spread uniformly in the droplets. As the continuous phase flowrate was further increased to 4.0 μL/min, it was observed that the droplet generation became unstable and the droplet size constantly varied. Therefore a high continuous phase flowrate was not suited for this case and thus a continuous phase flowrate between 1.0 and 3.0 μL/min was used. Also continuous droplet generation with all droplets having uniform magnetic NPs distribution was achieved with the final recipe.

3.2 Optimization of the Flowrate Parameters

Optimizing the flowrate parameters of the working fluids was vital in order to obtain monodisperse droplets and hence monodisperse Janus particles. Moreover, this optimization was also essential in order to ensure that the polymerization of the particles was completed before their collection at the outlet. For this purpose a number of experiments were performed so as to optimize the volumetric flowrates of the two working fluids; Q_d (volumetric flow rate of the dispersed phase fluid) and Q_c (volumetric flow rate of the continuous phase fluid). As the flowrate values were varied, the ratio D_d/D_h was calculated and plotted, where D_d is the droplet diameter and D_h is the hydraulic diameter given by $4A/P$, where A is the cross-sectional area of the orifice and P is the perimeter of the orifice.

In the first series of experiments Q_d was kept constant at 0.2 μL/min, whereas Q_c was varied from 0.2 to 3.0 μL/min. The observations were plotted using the flow rate fraction ϕ which is the ratio of Q_d to Q_c ($\phi = Q_d/Q_c$). The ratio D_d/D_h varied from 0.58 to 0.78 in this case.

In the beginning when Q_c was varied between 3.0 and 1.3 μL/min ($0.067 < \phi < 0.15$), the increase in the ratio D_d/D_h is substantial which is because of the droplet generation occurring in the dripping regime. In the dripping regime the droplet generation is dependent on the shear forces and the interfacial forces are

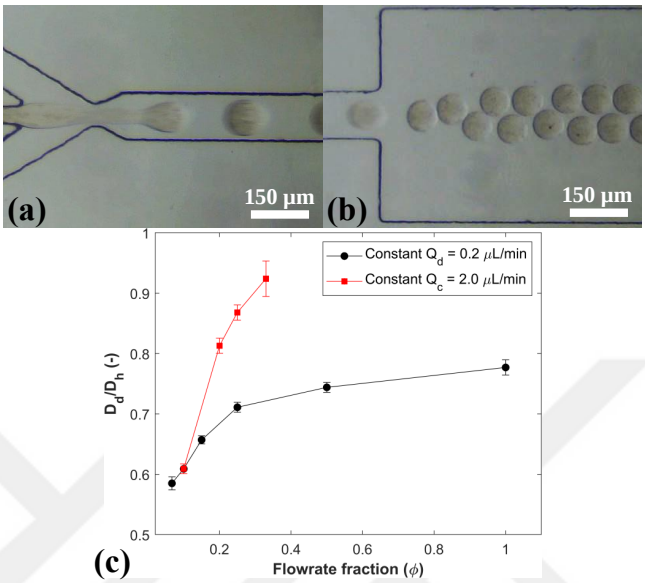

Figure 3.7: (a) Optical microscope image of the droplet generation at the junction. (b) Droplets flow into the wider channel downstream. (c) Variation of D_d/D_h at different flow rates of the continuous phase (Q_c) and the dispersed phase (Q_d), where D_d is the droplet diameter and D_h is the hydraulic diameter. D_h is given by $4A/P$, where A is the cross-sectional area of the orifice and P is the perimeter of the orifice. Note: Reprinted with permission from Saqib, Muhammad, Batur Ercan, and E. Yegan Erdem. "Synthesis of Anisotropic Magnetic Polymeric Janus Particles by In Situ Separation of Magnetic Nanoparticles in a Microfluidic Device." Langmuir 39.48 (2023): 17080-17087. Copyright 2023 American Chemical Society [84].

negligible. Figures 3.7 (a) and (b) demonstrate an example of droplet generation taking place in the dripping regime. As Q_c increases further the ratio D_d/D_h increases as well however this increase is gradual which is because of the transition of the droplet generation to the squeezing regime ($\phi > 0.25$). In the squeezing phase, droplets are generated due to pressure difference between the upstream and downstream of the channel. This difference is caused by the partial or full blockage of the main channel by the leading edge of the dispersed phase stream. Moreover when Q_c was further reduced, the ratio D_d/D_h increased however it started to become constant at a Q_c value of 0.2 μL/min ($\phi = 1$) which is because of the dispersed phase stream continuously elongating inside the main channel as the droplet generation proceeds further in the squeezing regime. Figures 3.8 (a) and (b) show the droplet generation in case of two values of ϕ (0.5 and 1) in

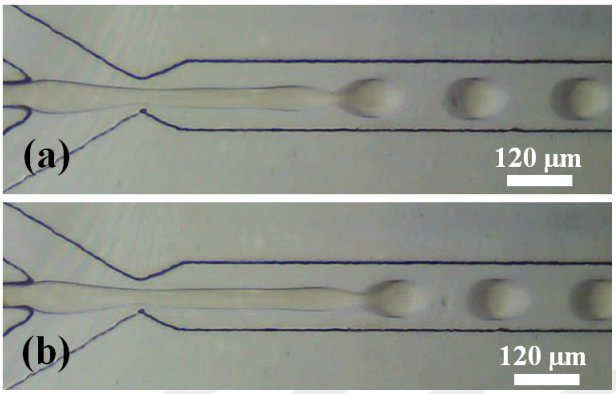

Figure 3.8: Droplet generation in the squeezing regime (a) ϕ=0.5. (b) ϕ=1.0. Note: Reprinted with permission from Saqib, Muhammad, Batur Ercan, and E. Yegan Erdem. "Synthesis of Anisotropic Magnetic Polymeric Janus Particles by In Situ Separation of Magnetic Nanoparticles in a Microfluidic Device." Langmuir 39.48 (2023): 17080-17087. Copyright 2023 American Chemical Society [84].

the squeezing regime. On close observation it is revealed that the length of the dispersed phase stream was almost half as much in case of the dripping regime as it was in the case of the squeezing regime [86]. Further higher values of Q_c were not used to produce droplets because of the unstable hydrodynamic pressure of PEGDA prepolymer phase [87].

Further experiments were performed to study the effect of Q_d by varying it from 2.0 and 0.2 μL/min while keeping Q_c constant at 2.0 μL/min. In this case the ratio D_d/D_h varied between 0.60 and 0.92 with a very small change in Q_d. At high flow rate values of Q_d from 1.0 to 2.0 μL/min ($0.5 < \phi < 1$) the droplet generation did not take place and the dispersed phase stream kept flowing along the entire length of the channel. At lower flow rate values between 0.2 and 0.66 μL/min ($0.1 < \phi < 0.33$) the ratio D_d/D_h increased considerably with a small increase in Q_d as shown in Figure 3.7 (c). Thus, in order to generate uniform droplets, Q_c was selected as 2.0 μL/min and Q_d was selected as 0.2 μL/min with $\phi = 0.1$, which corresponds to the dripping regime. The error bars are evaluated by measuring the size of five consecutive droplets and finding their average and their standard deviation.

The capillary number Ca for this case was calculated as 0.017 using equation 3.1. The viscosity of the dispersed phase stream is calculated as 0.0313 Ns/m^2 using the gambill method [71]. The velocity of the continuous phase fluid is 2.775 mm/s and the interfacial tension between the dispersed phase fluid and the continuous phase fluid is 5.0 mN/m This shows that the droplet generation is indeed in the dripping regime and that it is governed by the shear force applied by the continuous phase fluid on the dispersed phase stream [88].

$$Ca = \frac{\mu U}{\gamma} \tag{3.1}$$

At this flow rate combination the average droplet size is 50.6 ± 0.5 μm and the average particle size after polymerization is 45.7 ± 1.6 μm. The decrease in size is attributed to the shrinkage due to polymerization.

3.3 Optimization of the Magnetic Flux Density

In the experimental setup, a droplet-based microfluidic device was utilized to generate prepolymer phase droplets, a permanent magnet was used to obtain compartmentalization of the magnetic nanoparticles in the droplets and a UV lamp (with an excitation wavelength of 395 nm) was used to initiate polymerization of the droplets into Janus particles [84]. A continuous phase fluid physically interacted with the dispersed phase fluid and applied shear force on it and segmented it into droplets. The continuous phase fluid also acted as a carrier medium to transport the droplets along the channel length and upto the outlet port. The magnetic flux density of the external magnetic field played an important role in the compartmentalization and hence the anisotropy of the magnetic Janus particles. For this reason it was important to identify the most appropriate magnet that would be used for this purpose. In the three cases described in the following subsections three different types of permanent magnets have been described and the experimental observations obtained have been noted.

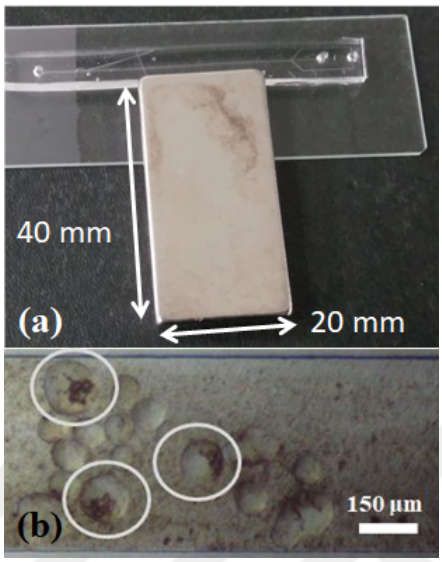

Figure 3.9: (a) Permanent magnet placed beside the device. (b) Droplets having accumulated nanoparticles due to the presence of the magnet.

In the first case the magnet used was a $40mm \times 20mm \times 5mm$ neodymium magnet. The experiments were performed with monomer solution as the dispersed phase (Figure 3.9 (a)); the direction the magnetic field was downwards. As a result the magnetic NPs clearly started to accumulate in part of the droplet (towards the magnetic field) as pointed in Figure 3.9 (b). But due to the instability in dispersed phase flow owing to the interference of the magnetic field, the droplet size was non-uniform.

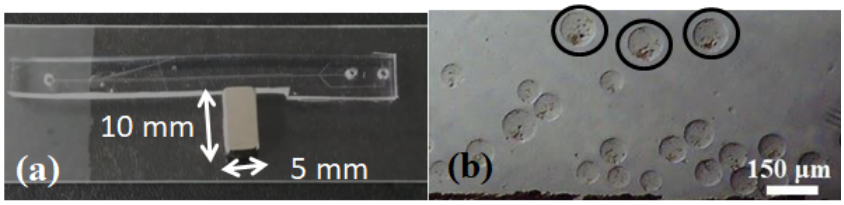

Figure 3.10: (a) Permanent magnet placed beside the device. (b) Droplets having accumulated nanoparticles due to the presence of the magnet.

From the previous experiment it was observed that the permanent magnet used had such a strong magnetic flux density that it was interfering with the droplet generation. For this reason in the second case the magnet used was a $10mm \times 5mm \times 5mm$ neodymium magnet Figure 3.10 (b). Because of the use of a smaller magnet with a lower magnetic flux density, the system kept

generating magnetically asymmetric droplets which could then be polymerized to form asymmetric polymer microparticles. But the nanoparticle accumulation was not definite as some droplets clearly showed magnetic separation while others did not (Figure 3.10 (b)).

The observations from the previous section indicated that the length of the magnetic flux application was not sufficient in order to make all droplets magnetically asymmetric. Due to this the length of the magnetic force application was increased from $5mm$ to $10mm$ (Figure 3.11 (a)) by placing an identical magnet by its side and therefore the system kept generating magnetically asymmetric droplets, as shown in Figure 3.11 (b). In these experiments the use of only PEGDA 575 as the monomer phase along with surfactant Tween 20 resulted in the magnetic nanoparticles being spread uniformly inside the droplets as shown in Figure 3.11 (c) after the removal of the magnet. This not only signifies that the magnet does not interfere with the droplet generation process but also that the homogeneity of the dispersed phase mixture caused the droplet shape and size to remain uniform.

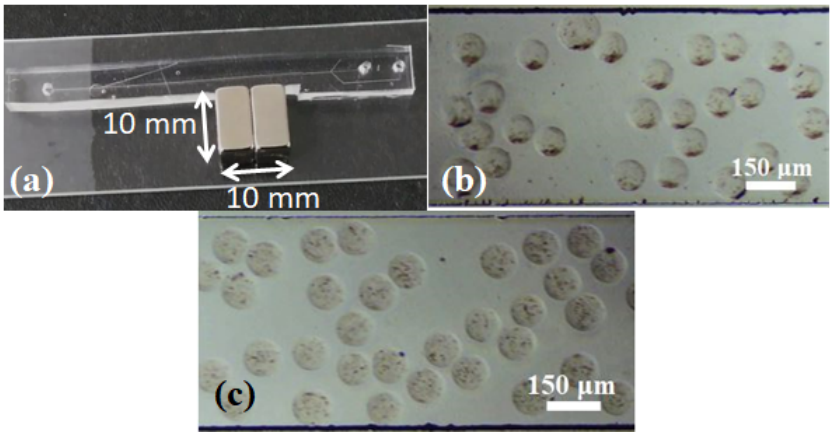

Figure 3.11: (a) Permanent magnet placed beside the device. (b) Droplets having accumulated nanoparticles due to the presence of the magnet. (c) Optical microscope image of droplets after magnetic field removal.

The magnetic nanoparticles utilized in the experiments were synthesized using the co-precipitation method in our laboratory. The magnetic nanoparticles were analyzed in a vibrating sample magnetometer so as to investigate their magnetic properties. In a vibrating sample magnetometer the specimen is vibrated inside

a uniform magnetic field to measure its magnetic moment. As a result of this vibration an electric current is produced and hence a voltage is generated in the sensing coils. The value of this voltage is determined by the magnetic moment of the sample. The magnetization data for the synthesized nanoparticles obtained from the vibration sample magnetometer is shown in Figure 3.12 (a). In the figure it can be observed that the slope of the magnetization curve is steep prior to 0.3 T, and later the specific magnetization of the magnetic nanoparticles begins to plateau and does not experience a significant rise in its value even with a significant increase in the applied magnetic field. Furthermore, as it can be seen from the figure there is no hysteresis in the magnetization curve which signifies that the nanoparticles are indeed superparamagnetic therefore from this point on these magnetic nanoparticles will be refered to as superparamagnetic iron oxide nanoparticles (SPIONs). This magnetization data was extremely important in evaluating what sort of magnet could be used in order to compartmentalize the SPIONs and also in ascertaining the distance of the magnet from the microfluidic channel.

By utilizing the data from the magnetization curve, experiments were performed so as to optimize the magnetic flux density inside the microfluidic channel. The range of values of the magnetic flux density that were studied were:

- smaller than 0.3 T
- equal to 0.3 T
- higher than 0.3 T

A pair of two neodymium magnets each with a height of 4mm, a length of 10mm and a width of 5mm were used to provide the magnetic field used in the experiments. The two magnets are placed besides each other and the 5mm edge is placed parallel to the microfluidic channel. The color intensity map of the magnetic flux density was plotted by making use of the formulae from Camacho et al. and the MATLAB functions from Cebron et al. [89, 90]. The magnetic flux density map is shown in Figure 3.12 (b). Since the magnetic flux density

is the strongest near the poles the microfluidic chip was placed in such a way that the wider channel was positioned perpendicular to the magnet. In this way as the droplets flow along the length of the channel, the magnetic field attracts the SPIONs that are encapsulated in the prepolymer phase droplets. The placement of the microfluidic chip with respect to the edge of the magnet is shown in Figure 3.12(b). The color intensity shows that the magnetic flux density inside the microchannel is around 0.3T. A magnetic flux density of such an order of magnitude does not result in any notable thermal effects [91].

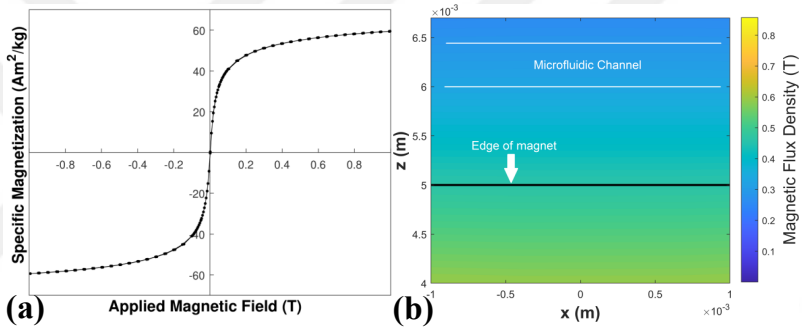

Figure 3.12: (a) Magnetization curve (T=300K) of dried magnetite nanoparticles. (b) Magnetic flux density map inside the microfluidic channel. Note: Reprinted with permission from Saqib, Muhammad, Batur Ercan, and E. Yegan Erdem. "Synthesis of Anisotropic Magnetic Polymeric Janus Particles by In Situ Separation of Magnetic Nanoparticles in a Microfluidic Device." Langmuir 39.48 (2023): 17080-17087. Copyright 2023 American Chemical Society [84].

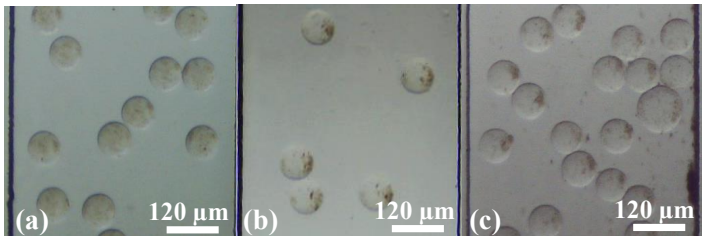

Figure 3.13: (a) Low magnetic flux density $< 0.3\ T$. (b) Optimum magnetic flux density: $0.3\ T$. (c) High magnetic flux density $> 0.3\ T$. Note: Reprinted with permission from Saqib, Muhammad, Batur Ercan, and E. Yegan Erdem. "Synthesis of Anisotropic Magnetic Polymeric Janus Particles by In Situ Separation of Magnetic Nanoparticles in a Microfluidic Device." Langmuir 39.48 (2023): 17080-17087. Copyright 2023 American Chemical Society [84].

As discussed earlier the droplets were generated in the dripping regime, in

which case the formation of the droplets is driven by the shear forces and the influence of the interfacial forces is negligible [92]. In droplet based microfluidics mixing of the contents inside the droplets is enhanced because of the chaotic advection. This chaotic advection is produced as a result of the immiscible interface at the boundary of the continuous and dispersed phases. In the case of a droplet flowing in an immiscible carrier fluid the velocity profile of the continuous phase fluid is altered because of the immiscibility of the two fluids. As a result of this altered flow profile of the continuous phase fluid, the droplets experience recirculation zones. In this particular experiment the recirculation zones present in the droplets lead to constant mixing of the SPIONs inside the droplets which caused the SPIONs to be evenly distributed. In order to compartmentalize the SPIONs to one hemisphere of the droplet, a magnetic force had to be applied. The value of the magnetic flux density was crucial in attaining the required anisotropy for the Janus particles. A low value of magnetic flux density resulted in the SPIONs spreading uniformly inside the droplet, as shown in Figure 3.13 (a). Similarly, a high magnetic flux density resulted in the SPIONs overcoming the interfacial tension and ultimately escaping the droplet, as shown in Figure 3.13 (c). The distance of the edge of the magnet to the microchannel was adjusted to maintain a magnetic flux density of 0.3 T and in this case the SPIONs agglomerated in one hemisphere as shown in Figure 3.13 (b). Accordingly, a magnetic flux density of 0.3 T was used in the experiments [84].

Chapter 4

Experimental Results

The Janus particles were synthesized using the experimental methodology explained in the previous chapter. After the synthesis it was important to characterize the Janus particles by using different characterizations tools. For this purpose the Janus particles were imaged under the optical microscope and their size distribution was calculated. Furthermore the particles were observed under the scanning electron microscope (SEM) to confirm that the particles had undergone complete polymerization. The particles were also observed in the presence of a permanent magnet so as to note their magnetic motion.

4.1 Synthesis of plain polymer particles

In the beginning plain polymer particles without any SPIONs were synthesized so as to test the polymerization setup. In case of the serpentine geometry, the droplet generation velocity was the same as the droplet transportation velocity due to which this device was prone to be affected by small inconsistencies in the flow rate of the liquids which caused the droplet train sequence, shown in Figure 2.9, to be disturbed and in turn resulted in non-uniform size and shape of the polymer particles as shown in the SEM image in Figure 4.1.

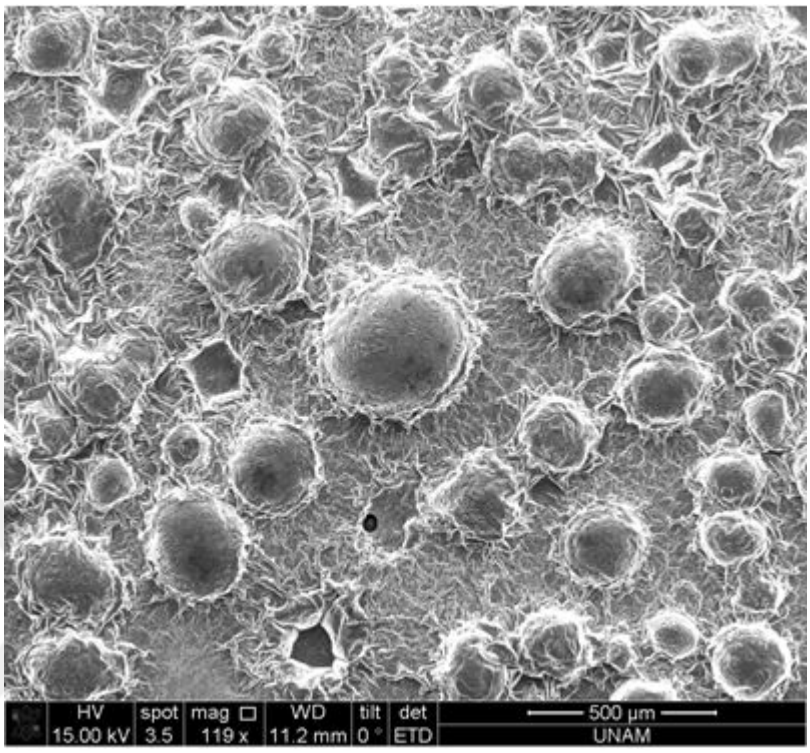

Figure 4.1: Scanning electron microscope image of the polymer particles synthesized by serpentine geometry.

The size distribution and shape of the particles was much better in the case of wider geometry, as it can be seen in the SEM image in Figure 4.2. There were still some irregularities in the shape caused by insufficient oil removal from the sample.

The SEM image in Figure 4.2 shows that there are spherical particles having a diameter of around 80 μm but there were still a lot of issues with the imaging, like particles with strange non-spherical shapes and image focusing problems. Figure 4.3 (a) is an optical microscope image of the particles after recovering them from the device and it clearly shows that the synthesized particles are originally spherical but their appearance becomes distorted due to the shortcomings in the SEM sample preparation process. Following are the solutions implemented in order to get rid of these problems:

- In order to eliminate non-spherical shaped particles, focus was shifted on

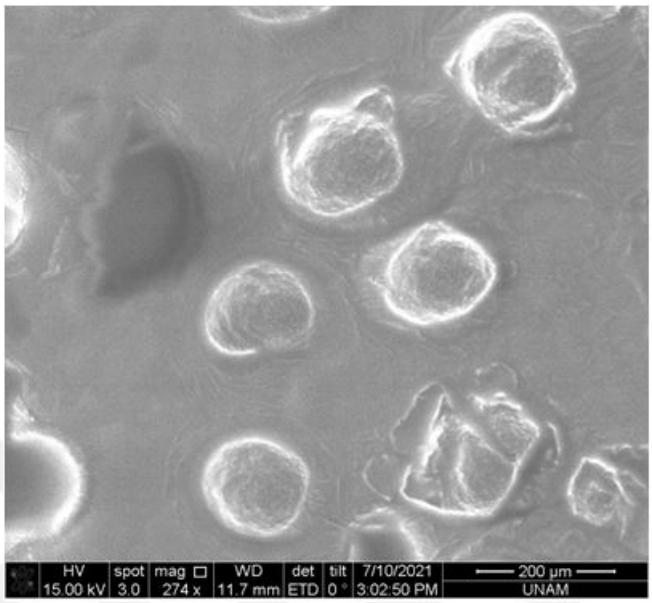

Figure 4.2: Scanning electron microscope image of the synthesized polymer particles synthesized by wider geometry.

proper oil and uncured monomer solution removal which could be achieved by washing with IPA (Isopropyl alcohol).

- The objects having an unusually large diameter are excess oil droplets that get coated by gold and are imaged under SEM as particles. Also the features of the conducting tape that is used for imaging particles might be shown as particles. For this reason the sample was prepared on a clean piece of Si wafer instead of conducting tape.

- Image focusing problems are related to oil removal and image settings of the SEM. In order to get better images SEM settings were optimized.

After taking these improvements into consideration, more samples were prepared and the corresponding SEM is shown in Figure 4.3 (b). It can be seen that the polymer microparticles (containing magnetic NPs) are monodispersed and have a diameter in the range 75-80 μm.

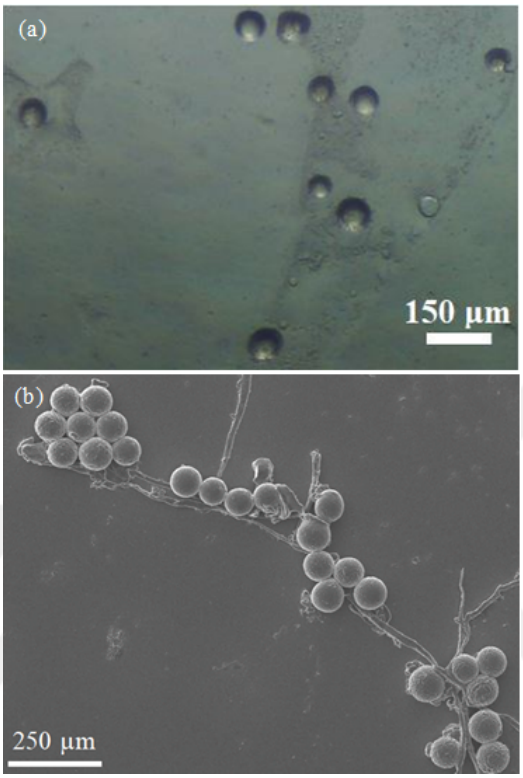

Figure 4.3: (a) Optical microscope image showing polymerized particles having a spherical shape. (b) Scanning electron microscope image of the synthesized polymer particles.

4.2 Synthesis of magnetically anisotropic Janus particles

4.2.1 Low Magnetic Fluid Concentration

In the beginning anisotropic magnetic Janus particles were synthesized using a ferrofluid having a concentration of 0.12 g/ml. After the droplets were polymerized, it was observed that the particles were monodisperse and were anisotropic as shown in Figure 4.4. The particles had a distinct magnetic hemisphere and a non-magnetic hemisphere.

Even though the particles appeared magnetically anisotropic, they did not exhibit any magnetic response to an external magnetic field. The scanning electron

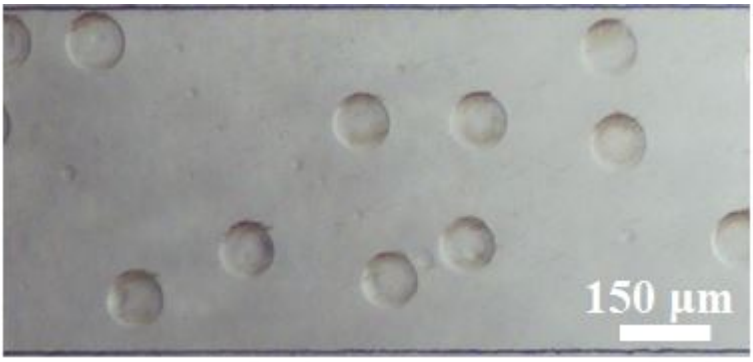

Figure 4.4: Optical microscope image of the Janus particles synthesized by using a low magnetic fluid concentration.

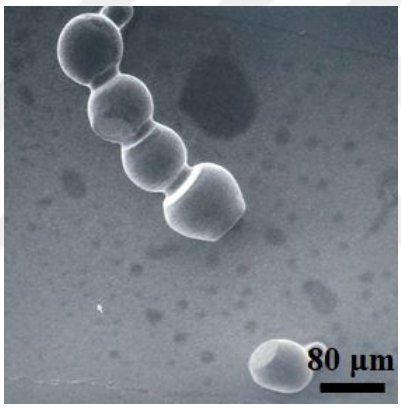

Figure 4.5: SEM image of the Janus particles synthesized by using a low magnetic fluid concentration.

microscope image of the polymer particles provided insight into the reason for no magnetic response. As shown in Figure 4.5, one hemisphere of the particles got teared away as the particles were washed with deionized water. This points to the fact that the magnetic part did not get polymerized along with the polymer particle due to which it got removed as it was washed.

4.2.2 High Magnetic Fluid Concentration

In order to ensure that the magnetic part stays intact after polymerization, the concentration of the SPIONs was increased to 0.25 g/ml. It was expected that by increasing the magnetic nanoparticle concentration, the water content of the

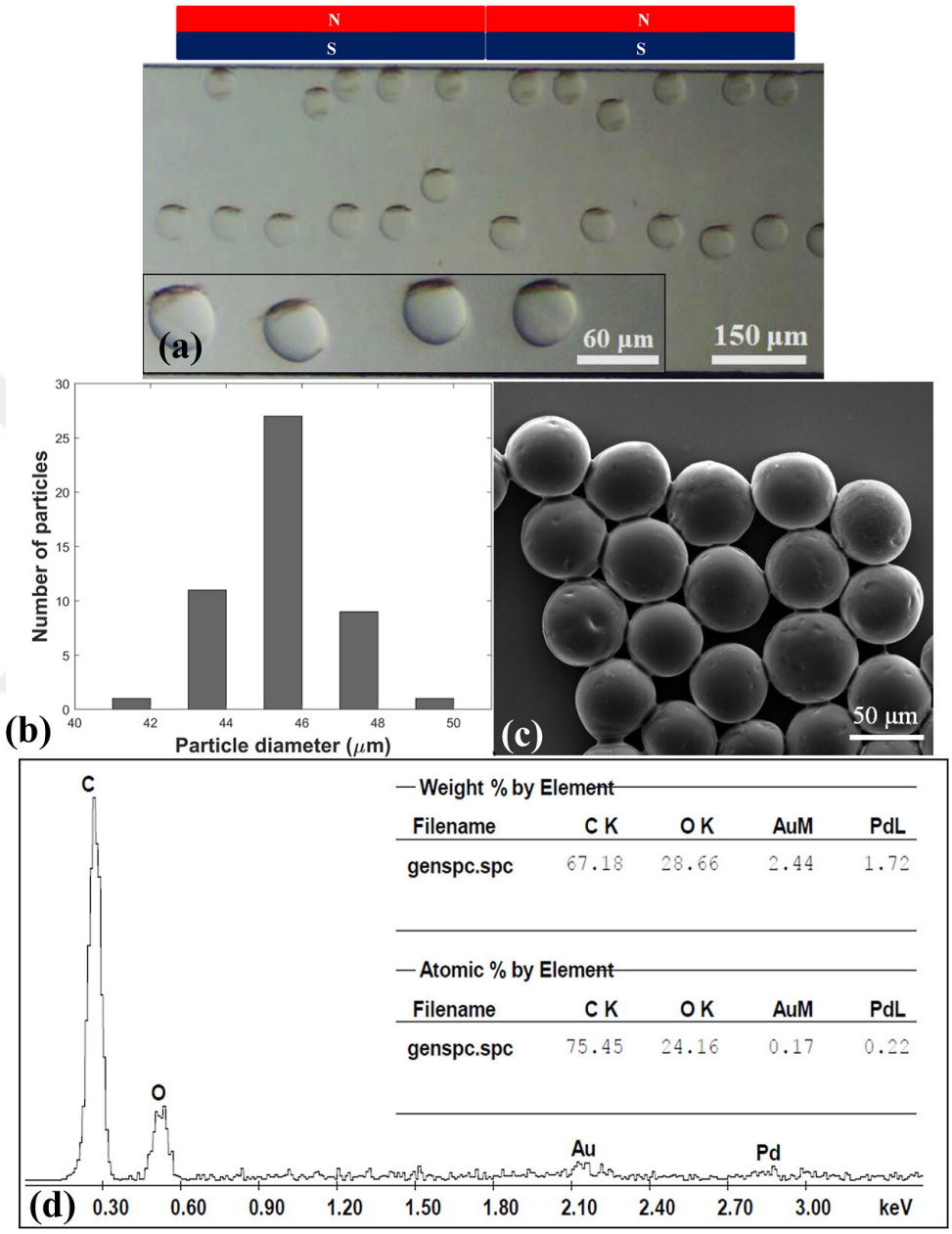

Figure 4.6: (a) Optical microscope image of the anisotropic magnetic Janus particles after polymerization within the microfluidic device. (b) Size distribution of the particles. (c) SEM image of the Janus particles. (d) EDX spectrum of the Janus particles. Note: Reprinted with permission from Saqib, Muhammad, Batur Ercan, and E. Yegan Erdem. "Synthesis of Anisotropic Magnetic Polymeric Janus Particles by In Situ Separation of Magnetic Nanoparticles in a Microfluidic Device." Langmuir 39.48 (2023): 17080-17087. Copyright 2023 American Chemical Society [84].

droplet could be decreased leading to a higher concentration of the monomer solution in each droplet. Figure 4.6 shows an example of anisotropic magnetic particles that had their magnetic part intact.

The polymerized anisotropic magnetic Janus particles were imaged with an optical microscope as shown in Figure 4.6 (a) before collecting them at the outlet. A total of 50 random Janus particles were utilized to plot the size distribution of the particles. In addition the average diameter of the particles and their standard deviation were calculated as 45.7 µm and 1.6 µm respectively. The size distribution plot of the particles is shown in 4.6 (b) Furthermore the Janus particles were observed under a Scanning Electron Microscope (SEM) in order to ensure that the polymerization of the particles had occurred (Figure 4.6 (c)). According to the size measurements the Janus particles shrink by 9.7% in size because of polymerization. Moreover the EDX spectra (Figure 4.6 (d)) verifies that the spherical particles are comprised of PEGDA which is apparent from the Carbon and Oxygen peaks. These peaks are characteristic of PEGDA surfaces along with the obtained weight percentages [93]. In order to understand if the 9.7% shrinkage in size was related to the dispersion of the prepolymer fluid into the continuous phase fluid an experiment was performed in which the continuous phase fluid and prepolymer phase fluid were added in a predetermined volume to a centrifuge tube and the contents were mixed thoroughly. After the mixture was allowed to settle down, the prepolymer phase fluid settled to the bottom of the centrifuge tube and its volume did not change from its original volume. This showed that the prepolymer phase did not disperse into the continuous phase fluid and that the entire shrinkage was indeed due to the polymerization.

4.2.3 Magnetic Response of the Janus Particles

A permanent magnet was placed adjacent to the device so as to observe the magnetic response of the Janus particle. The standard reaction of magnetically anisotropic materials to an external magnetic field is rotation about their own

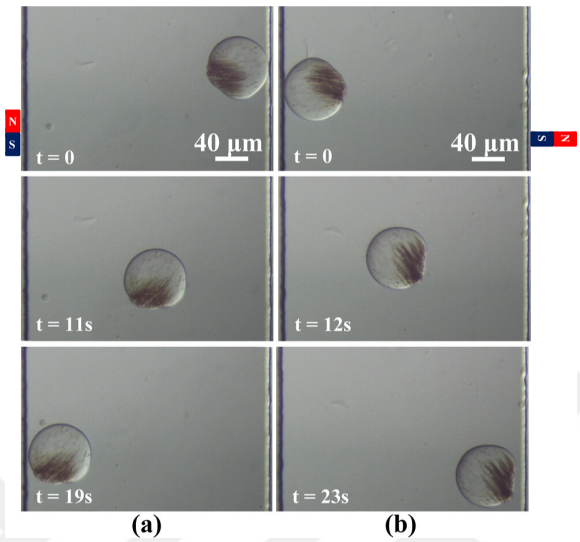

Figure 4.7: (a) An anisotropic magnetic Janus particle rotates in counter-clockwise direction while moving towards the direction of the magnetic field. (b) An anisotropic magnetic Janus particle rotates in the clockwise direction while moving towards the direction of the magnetic field. Note: Reprinted with permission from Saqib, M., Ercan, B., & Erdem, E. Y. (2023). Synthesis of Anisotropic Magnetic Polymeric Janus Particles by In Situ Separation of Magnetic Nanoparticles in a Microfluidic Device. Langmuir, 39(48), 17080-17087. Copyright 2023 American Chemical Society [84].

axis. This is the defining difference between magnetically isotropic and magnetically anisotropic particles. This rotation about its own axis is due to the unbalanced magnetic torque experienced by the particle's magnetic hemisphere because the non-magnetic part does not experience any magnetic torque. The Janus particle was made to rotate in the counter-clockwise direction (Figure 4.7 (a)), and in the clockwise direction (Figure 4.7 (b)). This trial was carried out while the Janus particle was present in the continuous phase fluid. During this rotation motion it was also observed that the particle translated along the width of the microfluidic channel.

It is observed that the particle rotated in the counter-clockwise direction, in the beginning, and later as its magnetic part aligns with the magnetic field direction the particle translates along the channel width. As a result of this translational motion, the particle covered a distance of 500 μm (from right to left) along a diagonal path with an average velocity of 33.3 μm/s. Likewise in Figure 4.7 (b)

the particle rotated in the clockwise direction followed by a translational motion along a diagonal path covering a distance of 517 μm with an average velocity of 21.5 μm/s. The direction of the magnetic field can be varied in order to change the orientation of the magnetic part and to translate and rotate the particle in a specific direction.

The maximum angular velocity (ω_{max}) of the particle when placed in an external magnetic flux is given by equation 4.1, where B is the magnetic flux density of the external magnet, m is the magnetic moment of the particle which is given by the equation 4.2, V is the volume of the magnetic part, M is the magnetization which is given by equation 4.3, M_s is the saturation magnetization of the SPIONs, μ_c is the magnetic permeability of the continuous phase fluid, a is the distance between the geometric center of the particle and its magnetic center, η is the viscosity of the continuous phase fluid and D is the particle diameter.

$$\omega_{max} = \frac{mB}{3\pi a^2 \eta D} \tag{4.1}$$

$$m = V \times M \tag{4.2}$$

$$M = \frac{M_s}{\mu_c} \tag{4.3}$$

Substituting all the values in the equation 4.1:

- B = 0.3 T
- M_s = 5.5 mT
- $\mu_c = 1.26 \times 10^{-6}$ mkgs^{-2}A^{-2}
- V = 2.39×10^{-14} m^3
- a = 11.4 μm

- $\eta = 0.0313$ Pa.s
- D = 45.7 μm

$\omega_{max} = 2.8$ kHz

A sample of 50 random particles was observed to determine how many of the synthesized particles are magnetically anisotropic. A total of 42 particles were magnetically anisotropic and the other 8 particles either did not contain any SPIONs or did not have compartmentalization of the SPIONs in one hemisphere. Therefore 84% of the particles were determined to be magnetically anisotropic.

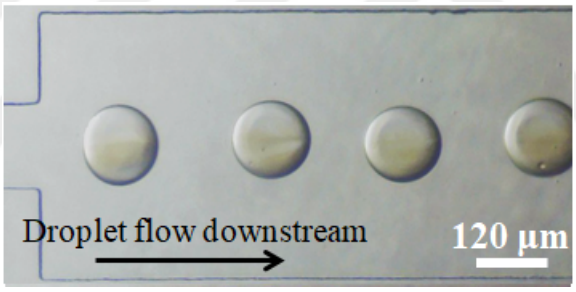

Figure 4.8: After coalescence Fe_2O_3/TiO_2 Janus droplets are transported downstream in the wider channel.

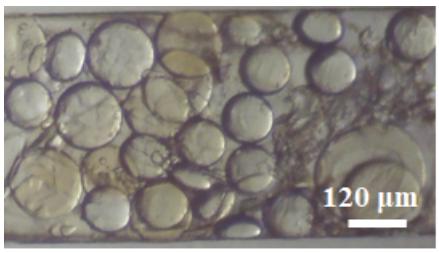

Figure 4.9: Optical microscope images of the Fe_2O_3/TiO_2 Janus particles.

4.3 Synthesis of Fe_2O_3/TiO_2 Janus particles

Experiments were performed to utilize the asymmetric cross-junction geometry for Janus particle synthesis using monomer solutions mixed with SPIONs (brown

coloured) and titanium dioxide nanoparticles (white coloured) as the two dispersed phases. It can be clearly seen that the two semicircular parts of the droplet are clearly distinct from each other giving the droplet its Janus configuration. The merged droplets then continue to flow in the wider channel in a synchronized manner while maintaining the Janus configuration as shown in Figure 4.8. At the same time a UV lamp, placed on the device, exposes the droplets to UV radiation which initiates polymerization of the droplets into solid particles due to the presence of photo-initiator in the dispersed phase. The average size of particles calculated from the experiments was 95.4 ± 1.4 μm. The optical microscope image of the Janus particles is shown in Figure 4.9. The synthesized Fe_2O_3/SiO_2 Janus particles are imaged under SEM as shown in Figure 4.10. The EDX spectra, shown in the figure confirm that the particles observed under are indeed PEGDA polymer particles since the EDX is characteristic of PEGDA.

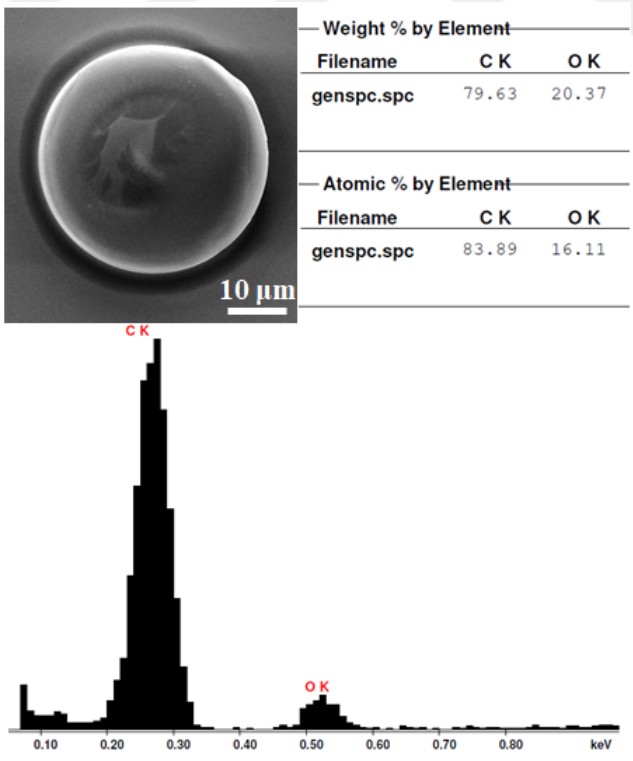

Figure 4.10: SEM image of the synthesized Janus particle and the corresponding EDX data of the synthesized Fe_2O_3/TiO_2 Janus particles.

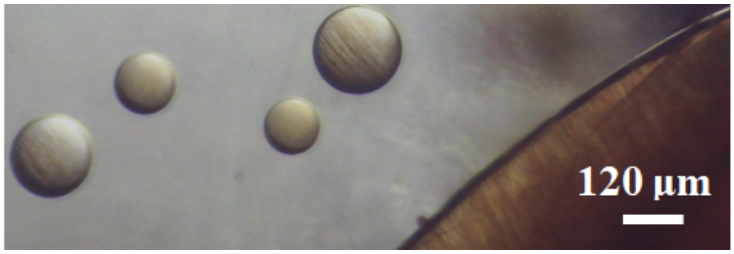

Figure 4.11: Optical microscope images of the Fe_2O_3/SiO_2 Janus particles.

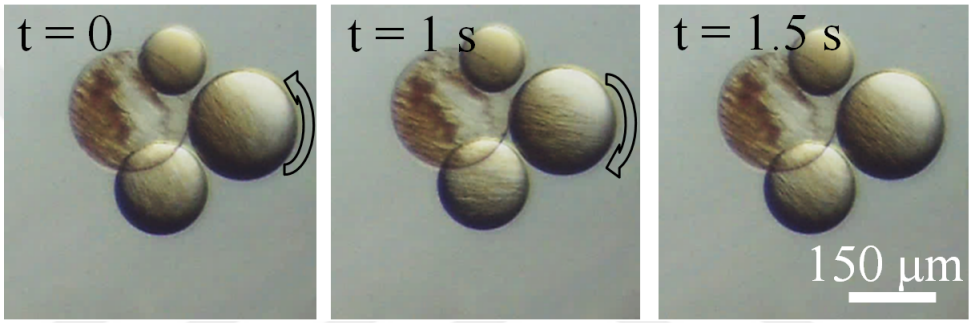

Figure 4.12: Magnetic response of the synthesized Fe_2O_3/SiO_2 Janus particle.

4.4 Synthesis of Fe_2O_3/SiO_2 Janus particles

The asymmetric cross-junction device was used to synthesize Fe_2O_3/SiO_2 Janus particles. Two dispersed phase inlets were utilized to deliver the two phases to the main channel. The first droplet was sheared by the continuous phase flow and it reached the second droplet generation junction as the other droplet was being generated. The droplets merged in the Janus orientation due to the controlled angle of merging. The merged Janus droplets were transported downstream and maintained their Janus composition due to the uniform flow conditions and meanwhile exposure to UV radiation caused the polymerization of the Janus droplets to particles. The optical microscope image of the Janus particles (Figure 4.11) shows the two distinct hemispheres in the particles. One of the hemispheres contains brown colored SPIONs and the other contains the SiO_2 nanoparticles.

4.4.1 Magnetic Response of the Fe_2O_3/SiO_2 Janus particles

The most important characteristic of a magnetically anisotropic particle is the ability to rotate about its own axis and is also used as a confirmation for its magnetic anisotropy [54, 66, 94]. While monophase particles can only traverse in a straight line, magnetically anisotropic particles have the ability to rotate about their own axis. This ability stems from the absence of magnetic moment on one hemisphere of the particle. As the particle is placed in an external magnetic flux, the magnetic part experiences a magnetic moment due to the interaction of the magnetic field. This magnetic moment is absent for the case of the non-magnetic hemisphere since there is no magnetic material present. Consequently the particle experiences a resultant magnetic torque which causes the particle to rotate about its own axis.

In order to observe this anisotropic characteristic of the synthesized Fe_2O_3/SiO_2 Janus particles a permanent magnet was placed beside it and the rotation of the particle was observed. Figure 4.12 shows how the magnetic Janus particle responds to the magnetic field. Initially the particle is stationary and as the permanent magnet is brought closer to it the particle rotates in a counter-clockwise direction and as the magnet is moved to the opposite direction the magnetic part of the particle follows the magnet and rotates in the clockwise direction. The important thing to note is that the position of the SPIONs does not change inside the particle which also verifies the fact that the particle has undergone complete polymerization.

Chapter 5

Conclusions and Future Work

In this work a microfluidic device for the synthesis of magnetically anisotropic Janus particles was reported. Janus particles are known to provide multi-functionality and orientation dependent physical and chemical properties that are much superior to conventional isotropic particles. The microfluidic device comprises a droplet generation junction (flow-focusing geometry), a wider channel downstream where the droplets are slowed down due to the change in the cross-sectional area while at the same time being exposed to an external magnetic field for the compartmentalization of magnetic nanoparticles and an ultraviolet lamp for the polymerization of the prepolymer phase droplets into solid particles. The droplet generation junction design was optimized to generate uniform droplets at a high frequency using numerical simulations and experimental results. The recipe of the dispersed phase, which contained a prepolymer phase Polyethyleneglycol diacrylate (PEGDA), was optimized to ensure continuous uniform droplet generation. The continuous phase fluid was optimized as well to ensure that the interfacial tension between the two phases was increased. As a result of these optimization processes continuous uniform droplet generation of PEGDA containing magnetic nanoparticles was achieved. It was also observed that the low viscosity PEGDA 575 was better at uniformly dispersing the SPIONs compared to the high viscosity PEGDA 700. The non-uniform dispersion of SPIONs in the dispersed phase not only reduced the quality of the synthesized Janus particles it

also caused clogging o the channels resulting in non-uniform droplet generation and hence particles with a wide size distribution which is not desirable. After the droplet genration at the droplet generation junction the droplets were transported into the wider channel their velocity reduced and they were influenced by the external magnetic field to ensure that all magnetic nanoparticles accumulate into one hemisphere of the droplet. The external magnetic flux density was optimized by using the magnetization data of the magnetic nanoparticles which revealed that the nanoparticles were superparamagnetic and by using a magnetic flux density map. The magnetic flux density value was selected as 0.3 T and when used in the experiments it brought about the required compartmentalization of the superparamagnetic iron oxide nanoparticles (SPIONs). A magnetic flux density value less than that did not create magnetic separation and a value greater than that caused the SPIONs to escape the droplets. In terms of the geometry of the downstream channel, it was observed that a serpentine geometry was not suitable since it did not reduce the velocity of the droplets and often droplets merged while polymerization causing the microchannel to get clogged. Hence a wider channel was used to slow down the droplets and allow for complete polymerization. The Janus particles were imaged under an optical microscope and their size distribution was plotted using 50 random particles. The particles were collected at the outlet and washed with isopropyl alcohol to remove excess oil and later they were imaged under SEM to ensure that they had undergone complete polymerization. Motion experiments were also performed in order to observe the motion of the Janus particles under an external magnetic field. It was observed that a sample Janus particle not only rotated in the direction of the external field but also translated in its direction. The rotation of the particle was the result of its magnetic anisotropy due to the net magnetic moment on the magnetic part.

Another device for the synthesis of Janus particles having two types of nanoparticles in each hemisphere was designed. Among the designs tested for merging efficiency the asymmetric cross-junction device was observed to be the most efficient in continuous generation of Janus droplets. The prepolymer phase was highly PEGDA 700 in this case and therefore genrating continuously uniform droplets was not possible without decreasing the viscosity of the dispersed phase

which was achieved by mixing deionized water. The addition of deionized water reduced the viscosity of the dispersed phase and resulted in the generation of continuously merging uniform droplets. The microfluidic device was an asymmetric cross-junction geometry having an expanded section to facilitate the merging of droplets. The distance between the two asymmetric droplet junctions was fixed in such a way that the first droplet approached the second droplet just as it got pinched off from its dispersed phase stream. The separation of the contents of the two hemispheres was achieved by having the droplets merge in a sideways orientation instead of a head-on orientation. The angle of merging was the deciding factor in maintaining the Janus orientation of the droplets. As the droplets were transported further downstream the contents of the two hemispheres remained separated due to the fact that chaotic advection inside a droplet based device gives rise to recirculation zones that are generated along the symmetry of the microchannel in case of a uniform symmetric flow. During this time the droplets are exposed to UV radiation to initiate polymerization of the droplets into solid particles.The particles were then collected at the outlet and imaged under the optical microscope and under the scanning electron microscope. The obtained results show that the synthesized particles underwent complete polymerization and were magnetically anisotropic in nature. The particles were also placed in an external magnetic field to observe their magnetic motion. The motion experiment results reveal that the net magnetic torque causes the particles to rotate about their own axis which further verifies the anisotropy of the particles.

Recommendations for future work

There are some suggestions that could further add value to the final product.

- The asymmetric cross-junction device has been used with the same type of prepolymer phase from both dispersed phase inlets. This means that the resultant particle will have an overall hydrophilic nature since PEGDA is hydrophilic. This same device could be used to synthesize amphiphilic particles (particles with both hydrophobic and hydrophilic nature) by using a hydrophilic prepolymer phase from one inlet and using a hydrophobic prepolymer phase (like ethoxylated trimethylolpropane triacrylate (ETPTA)).

This would give increased functionality to the particles.

- This work presented a methdology to synthesize magnetically anisotropic Janus particles. The particles could be further chemically modified after synthesis to create pores on the surface of the polymeric particles. The pores on the surface of the polymeric Janus particles would not only improve the rate of bubble production in bubble-driven Janus micromotors but would also boost water-repellent properties of the hydrophobic portion of the Janus particle.

- The asymmetric cross-junction device has been used to synthesize Janus particles but it could potentially be used to synthesize core shell particles as well by tuning the interfacial tension values of the two dispersed phase fluids and by changing the spreading coefficient value that has been explained in detail in chapter 1. These core shell particles having a magnetic core could be potentially used for applications such as magnetic resonance imaging (MRI) due to their biocompatability.

This research presents a thorough investigation of the synthesis of magnetically anisotropic Janus polymer particles *via* droplet-based microfluidics techniques, marking a significant advancement in the field of materials science and nanotechnology. Through a combination of experimental methodologies and theoretical analysis, this research elucidates the intricate mechanisms governing the formation and properties of these unique particles, providing valuable insights into their potential applications in various scientific and technological domains. By making use of the principles of microfluidics, this research exhibits precise control over the particle morphology, composition, and magnetic properties, opening new horizons for the design and engineering of functional materials with customized characteristics. Furthermore, the novel synthesis approach developed in this thesis not only expands our fundamental understanding of particle synthesis at the microscale but also lays the foundation for future research endeavors aimed at exploring the diverse functionalities and applications of magnetically anisotropic Janus polymer particles.

Bibliography

[1] L. Zhang, K. Chen, H. Zhang, B. Pang, C.-H. Choi, A. S. Mao, H. Liao, S. Utech, D. J. Mooney, H. Wang, *et al.*, "Microfluidic templated multicompartment microgels for 3d encapsulation and pairing of single cells," *Small*, vol. 14, no. 9, p. 1702955, 2018.

[2] J. Lan, J. Chen, N. Li, X. Ji, M. Yu, and Z. He, "Microfluidic generation of magnetic-fluorescent janus microparticles for biomolecular detection," *Talanta*, vol. 151, pp. 126–131, 2016.

[3] T. Nisisako, T. Torii, T. Takahashi, and Y. Takizawa, "Synthesis of monodisperse bicolored janus particles with electrical anisotropy using a microfluidic co-flow system," *Advanced Materials*, vol. 18, no. 9, pp. 1152–1156, 2006.

[4] I. U. Khan, C. A. Serra, N. Anton, X. Li, R. Akasov, N. Messaddeq, I. Kraus, and T. F. Vandamme, "Microfluidic conceived drug loaded janus particles in side-by-side capillaries device," *International Journal of Pharmaceutics*, vol. 473, no. 1-2, pp. 239–249, 2014.

[5] H. Xie, Z.-G. She, S. Wang, G. Sharma, and J. W. Smith, "One-step fabrication of polymeric janus nanoparticles for drug delivery," *Langmuir*, vol. 28, no. 9, pp. 4459–4463, 2012.

[6] Z.-Q. Feng, K. Yan, J. Li, X. Xu, T. Yuan, T. Wang, and J. Zheng, "Magnetic janus particles as a multifunctional drug delivery system for paclitaxel in efficient cancer treatment," *Materials Science and Engineering: C*, vol. 104, p. 110001, 2019.

[7] K. D. Seo, J. Doh, and D. S. Kim, "One-step microfluidic synthesis of janus microhydrogels with anisotropic thermo-responsive behavior and organophilic/hydrophilic loading capability," *Langmuir*, vol. 29, no. 49, pp. 15137–15141, 2013.

[8] Y. Indalkar, S. Gaikwad, and A. Ubale, "Janus particles recent and novel approach in drug delivery: an overview," *Journal of Current Pharma Research*, vol. 3, no. 4, p. 1031, 2013.

[9] Z. Yang, D. A. Aarts, Y. Chen, S. Jiang, P. Hammond, I. Kretzschmar, H.-J. Schneider, M. Shahinpoor, A. H. Muller, C. Xu, *et al.*, *Janus particle synthesis, self-assembly and applications*. Royal Society of Chemistry, 2012.

[10] G. Song, M. Chen, Y. Zhang, L. Cui, H. Qu, X. Zheng, M. Wintermark, Z. Liu, and J. Rao, "Janus iron oxides@ semiconducting polymer nanoparticle tracer for cell tracking by magnetic particle imaging," *Nano letters*, vol. 18, no. 1, pp. 182–189, 2018.

[11] Z. Rahiminezhad, A. M. Tamaddon, S. Borandeh, and S. S. Abolmaali, "Janus nanoparticles: new generation of multifunctional nanocarriers in drug delivery, bioimaging and theranostics," *Applied Materials Today*, vol. 18, p. 100513, 2020.

[12] Y. Zhang, K. Huang, J. Lin, and P. Huang, "Janus nanoparticles in cancer diagnosis, therapy and theranostics," *Biomaterials science*, vol. 7, no. 4, pp. 1262–1275, 2019.

[13] T. NISISAKO, T. ANDO, and T. HATSUZAWA, "Biconvex polymer microlenses fabricated from microfluidic janus droplets," *Journal of the Japan Society for Precision Engineering*, vol. 79, no. 5, pp. 460–466, 2013.

[14] T. Nisisako, T. Ando, and T. Hatsuzawa, "Capillary-assisted fabrication of biconcave polymeric microlenses from microfluidic ternary emulsion droplets," *Small*, vol. 10, no. 24, pp. 5116–5125, 2014.

[15] T. Nisisako, H. Suzuki, and T. Hatsuzawa, "Biconvex polymer microlenses with tunable imaging properties designed by janus droplet microfluidics," *Micromachines*, vol. 6, no. 10, pp. 1435–1444, 2015.

[16] S.-H. Kim, S.-J. Jeon, W. C. Jeong, H. S. Park, and S.-M. Yang, "Optofluidic synthesis of electroresponsive photonic janus balls with isotropic structural colors," *Advanced materials*, vol. 20, no. 21, pp. 4129–4134, 2008.

[17] M. Guix, S. M. Weiz, O. G. Schmidt, and M. Medina-Sánchez, "Self-propelled micro/nanoparticle motors," *Particle & Particle Systems Characterization*, vol. 35, no. 2, p. 1700382, 2018.

[18] B. Jurado-Sánchez and J. Wang, "Micromotors for environmental applications: a review," *Environmental Science: Nano*, vol. 5, no. 7, pp. 1530–1544, 2018.

[19] A. Chen, X.-h. Ge, J. Chen, L. Zhang, and J.-H. Xu, "Multi-functional micromotor: microfluidic fabrication and water treatment application," *Lab on a Chip*, vol. 17, no. 24, pp. 4220–4224, 2017.

[20] M. Ren, W. Guo, H. Guo, and X. Ren, "Microfluidic fabrication of bubble-propelled micromotors for wastewater treatment," *ACS applied materials & interfaces*, vol. 11, no. 25, pp. 22761–22767, 2019.

[21] N. Safaie and R. C. Ferrier, "Janus nanoparticle synthesis: Overview, recent developments, and applications," *Journal of Applied Physics*, vol. 127, no. 17, 2020.

[22] A. M. Yake, C. E. Snyder, and D. Velegol, "Site-specific functionalization on individual colloids: Size control, stability, and multilayers," *Langmuir*, vol. 23, no. 17, pp. 9069–9075, 2007.

[23] Y. Zhang, L. Kang, H. Huang, and J. Deng, "Optically active janus particles constructed by chiral helical polymers through emulsion polymerization combined with solvent evaporation-induced phase separation," *ACS applied materials & interfaces*, vol. 12, no. 5, pp. 6319–6327, 2020.

[24] F. Jia, H. Li, R. Chen, and K. Zhang, "Self-assembly of dna-containing copolymers," *Bioconjugate Chemistry*, vol. 30, no. 7, pp. 1880–1888, 2019.

[25] M. M. Rahman, F. Montagne, H. Fessi, and A. Elaissari, "Anisotropic magnetic microparticles from ferrofluid emulsion," *Soft Matter*, vol. 7, no. 4, pp. 1483–1490, 2011.

[26] S.-Y. Teh, R. Lin, L.-H. Hung, and A. P. Lee, "Droplet microfluidics," *Lab on a Chip*, vol. 8, no. 2, pp. 198–220, 2008.

[27] D. J. Beebe, G. A. Mensing, and G. M. Walker, "Physics and applications of microfluidics in biology," *Annual review of biomedical engineering*, vol. 4, no. 1, pp. 261–286, 2002.

[28] V. Srinivasan, V. K. Pamula, and R. B. Fair, "An integrated digital microfluidic lab-on-a-chip for clinical diagnostics on human physiological fluids," *Lab on a Chip*, vol. 4, no. 4, pp. 310–315, 2004.

[29] Y. K. Suh and S. Kang, "A review on mixing in microfluidics," *Micromachines*, vol. 1, no. 3, pp. 82–111, 2010.

[30] C. N. Baroud, F. Gallaire, and R. Dangla, "Dynamics of microfluidic droplets," *Lab on a Chip*, vol. 10, no. 16, pp. 2032–2045, 2010.

[31] L. Shang, Y. Cheng, and Y. Zhao, "Emerging droplet microfluidics," *Chemical reviews*, vol. 117, no. 12, pp. 7964–8040, 2017.

[32] C. Marschelke, A. Fery, and A. Synytska, "Janus particles: from concepts to environmentally friendly materials and sustainable applications," *Colloid and Polymer Science*, vol. 298, pp. 841–865, 2020.

[33] M. Saqib, P. A. Tran, B. Ercan, and E. Y. Erdem, "Microfluidic methods in janus particle synthesis," *International Journal of Nanomedicine*, pp. 4355–4366, 2022.

[34] Z. Yu, C.-F. Wang, L. Ling, L. Chen, and S. Chen, "Triphase microfluidic-directed self-assembly: anisotropic colloidal photonic crystal supraparticles and multicolor patterns made easy," *Angewandte Chemie*, vol. 10, no. 124, pp. 2425–2428, 2012.

[35] X. Yu, C. Zhang, S. You, H. Liu, L. Zhang, W. Liu, S.-S. Guo, and X.-Z. Zhao, "Microfluidic synthesis of multiferroic janus particles with disk-like compartments," *Applied Physics Letters*, vol. 108, no. 7, 2016.

[36] T. Nisisako and T. Torii, "Formation of biphasic janus droplets in a microfabricated channel for the synthesis of shape-controlled polymer microparticles," *Advanced materials*, vol. 19, no. 11, pp. 1489–1493, 2007.

[37] M. Marquis, D. Renard, and B. Cathala, "Microfluidic generation and selective degradation of biopolymer-based janus microbeads," *Biomacromolecules*, vol. 13, no. 4, pp. 1197–1203, 2012.

[38] L. Cheng, B. Cai, Y. Zuo, L. Xiao, L. Rao, Z. He, Y. Yang, W. Liu, S. Guo, and X.-Z. Zhao, "Janus droplet parallel arrangements using a simple y-channel flow-focusing microfluidic device," *Chemical Physics Letters*, vol. 673, pp. 93–98, 2017.

[39] N. Pannacci, H. Bruus, D. Bartolo, I. Etchart, T. Lockhart, Y. Hennequin, H. Willaime, and P. Tabeling, "Equilibrium and nonequilibrium states in microfluidic double emulsions," *Physical review letters*, vol. 101, no. 16, p. 164502, 2008.

[40] R. F. Shepherd, J. C. Conrad, S. K. Rhodes, D. R. Link, M. Marquez, D. A. Weitz, and J. A. Lewis, "Microfluidic assembly of homogeneous and janus colloid-filled hydrogel granules," *Langmuir*, vol. 22, no. 21, pp. 8618–8622, 2006.

[41] S.-N. Yin, C.-F. Wang, Z.-Y. Yu, J. Wang, S.-S. Liu, and S. Chen, "Versatile bifunctional magnetic-fluorescent responsive janus supraballs towards the flexible bead display," *Advanced materials*, vol. 23, no. 26, pp. 2915–2919, 2011.

[42] T. Hessberger, L. B. Braun, F. Henrich, C. Müller, F. Gießelmann, C. Serra, and R. Zentel, "Co-flow microfluidic synthesis of liquid crystalline actuating janus particles," *Journal of Materials Chemistry C*, vol. 4, no. 37, pp. 8778–8786, 2016.

[43] K. P. Yuet, D. K. Hwang, R. Haghgooie, and P. S. Doyle, "Multifunctional superparamagnetic janus particles," *Langmuir*, vol. 26, no. 6, pp. 4281–4287, 2010.

[44] L. Zhao, L. Pan, K. Zhang, S. Guo, W. Liu, Y. Wang, Y. Chen, X. Zhao, and H. Chan, "Generation of janus alginate hydrogel particles with magnetic anisotropy for cell encapsulation," *Lab on a Chip*, vol. 9, no. 20, pp. 2981–2986, 2009.

[45] T. Nisisako, T. Torii, and T. Higuchi, "Novel microreactors for functional polymer beads," *Chemical Engineering Journal*, vol. 101, no. 1-3, pp. 23–29, 2004.

[46] S. Seiffert, M. B. Romanowsky, and D. A. Weitz, "Janus microgels produced from functional precursor polymers," *Langmuir*, vol. 26, no. 18, pp. 14842–14847, 2010.

[47] T. Kamperman, V. D. Trikalitis, M. Karperien, C. W. Visser, and J. Leijten, "Ultrahigh-throughput production of monodisperse and multifunctional janus microparticles using in-air microfluidics," *ACS applied materials & interfaces*, vol. 10, no. 28, pp. 23433–23438, 2018.

[48] Y. Liu and T. Nisisako, "Microfluidic generation of monodispersed janus alginate hydrogel microparticles using water-in-oil emulsion reactant," *Biomicrofluidics*, vol. 16, no. 2, 2022.

[49] J. Guzowski, P. M. Korczyk, S. Jakiela, and P. Garstecki, "The structure and stability of multiple micro-droplets," *Soft Matter*, vol. 8, no. 27, pp. 7269–7278, 2012.

[50] S. Torza and S. Mason, "Three-phase interactions in shear and electrical fields," *Journal of colloid and interface science*, vol. 33, no. 1, pp. 67–83, 1970.

[51] N. Prasad, J. Perumal, C.-H. Choi, C.-S. Lee, and D.-P. Kim, "Generation of monodisperse inorganic–organic janus microspheres in a microfluidic device," *Advanced Functional Materials*, vol. 19, no. 10, pp. 1656–1662, 2009.

[52] Y.-T. Yang, J. Wei, X. Li, L.-J. Wu, Z.-Q. Chang, and C. A. Serra, "A side-by-side capillaries-based microfluidic system for synthesizing size-and morphology-controlled magnetic anisotropy janus beads," *Advanced Powder Technology*, vol. 26, no. 1, pp. 156–162, 2015.

[53] K. Xu, X.-H. Ge, J.-P. Huang, Z.-X. Dang, J.-H. Xu, and G.-S. Luo, "A region-selective modified capillary microfluidic device for fabricating water–oil janus droplets and hydrophilic–hydrophobic anisotropic microparticles," *Rsc Advances*, vol. 5, no. 58, pp. 46981–46988, 2015.

[54] R. Al Nuumani, S. K. Smoukov, G. Bolognesi, and G. T. Vladisavljevic, "Highly porous magnetic janus microparticles with asymmetric surface topology," *Langmuir*, vol. 36, no. 42, pp. 12702–12711, 2020.

[55] J. Jeong, E. Um, J.-K. Park, and M. W. Kim, "One-step preparation of magnetic janus particles using controlled phase separation of polymer blends and nanoparticles," *RSC advances*, vol. 3, no. 29, pp. 11801–11806, 2013.

[56] X. Pang, C. Wan, M. Wang, and Z. Lin, "Strictly biphasic soft and hard janus structures: synthesis, properties, and applications," *Angewandte Chemie International Edition*, vol. 53, no. 22, pp. 5524–5538, 2014.

[57] R. K. Shah, J.-W. Kim, and D. A. Weitz, "Janus supraparticles by induced phase separation of nanoparticles in droplets," *Advanced Materials*, vol. 21, no. 19, pp. 1949–1953, 2009.

[58] S. Lone, S. H. Kim, S. W. Nam, S. Park, J. Joo, and I. W. Cheong, "Microfluidic synthesis of janus particles by uv-directed phase separation," *Chemical Communications*, vol. 47, no. 9, pp. 2634–2636, 2011.

[59] J. Kim, J. Joo, and S.-Y. Park, "Preparation of asymmetric porous janus particles using microfluidics and directional uv curing," *Particle & Particle Systems Characterization*, vol. 30, no. 11, pp. 981–988, 2013.

[60] W. Li, H. Dong, G. Tang, T. Ma, and X. Cao, "Controllable microfluidic fabrication of janus and microcapsule particles for drug delivery applications," *Rsc Advances*, vol. 5, no. 30, pp. 23181–23188, 2015.

[61] E. E. Ekanem, Z. Zhang, and G. T. Vladisavljevic, "Facile production of biodegradable bipolymer patchy and patchy janus particles with controlled morphology by microfluidic routes," *Langmuir*, vol. 33, no. 34, pp. 8476–8482, 2017.

[62] X. Wang, X. Feng, G. Ma, L. Yao, and M. Ge, "Amphiphilic janus particles generated via a combination of diffusion-induced phase separation and magnetically driven dewetting and their synergistic self-assembly," *Advanced Materials*, vol. 28, no. 16, pp. 3131–3137, 2016.

[63] X.-T. Sun, R. Guo, D.-N. Wang, Y.-Y. Wei, C.-G. Yang, and Z.-R. Xu, "Microfluidic preparation of polymer-lipid janus microparticles with staged drug release property," *Journal of colloid and interface science*, vol. 553, pp. 631–638, 2019.

[64] M. Xia, E. M. Go, K. H. Choi, J. H. Lim, B. Park, T. Yu, S. H. Im, S. K. Kwak, and B. J. Park, "One-step production of highly anisotropic particles via a microfluidic method," *Journal of Industrial and Engineering Chemistry*, vol. 64, pp. 328–336, 2018.

[65] C.-H. Chen, R. K. Shah, A. R. Abate, and D. A. Weitz, "Janus particles templated from double emulsion droplets generated using microfluidics," *Langmuir*, vol. 25, no. 8, pp. 4320–4323, 2009.

[66] C.-H. Chen, A. R. Abate, D. Lee, E. M. Terentjev, and D. A. Weitz, "Microfluidic assembly of magnetic hydrogel particles with uniformly anisotropic structure," *Advanced materials*, vol. 21, no. 31, pp. 3201–3204, 2009.

[67] J. Thiele and S. Seiffert, "Double emulsions with controlled morphology by microgel scaffolding," *Lab on a Chip*, vol. 11, no. 18, pp. 3188–3192, 2011.

[68] A. Perro, N. Coudon, J.-P. Chapel, N. Martin, L. Béven, and J.-P. Douliez, "Building micro-capsules using water-in-water emulsion droplets as templates," *Journal of Colloid and Interface Science*, vol. 613, pp. 681–696, 2022.

[69] M. Saqib, *Effect of Channel Geometry on Alternating Droplet Generation*. PhD thesis, Bilkent Universitesi (Turkey), 2018.

[70] S. L. Anna, N. Bontoux, and H. A. Stone, "Formation of dispersions using "flow focusing" in microchannels," *Applied physics letters*, vol. 82, no. 3, pp. 364–366, 2003.

[71] M. Druin and S. Kreps, "Prediction of viscosity of liquid hydrocarbons," *Industrial & Engineering Chemistry Fundamentals*, vol. 9, no. 1, pp. 79–83, 1970.

[72] C. Pozrikidis, "Creeping flow in two-dimensional channels," *Journal of Fluid Mechanics*, vol. 180, pp. 495–514, 1987.

[73] M. Saqib, O. B. Şahinoğlu, and E. Y. Erdem, "Alternating droplet formation by using tapered channel geometry," *Scientific reports*, vol. 8, no. 1, p. 1606, 2018.

[74] M. SAQIB and E. Y. ERDEM, "Generation of alternating droplets with different viscosities in a microfluidic channel," *Çukurova Üniversitesi Mühendislik Fakültesi Dergisi*, vol. 36, no. 3, pp. 791–798, 2021.

[75] F. Shen, Y. Li, G. Wang, and Z. Liu, "Mechanisms of rectangular groove-induced multiple-microdroplet coalescences," *Acta Mechanica Sinica*, vol. 33, pp. 585–594, 2017.

[76] K. Liu, H. Ding, Y. Chen, and X.-Z. Zhao, "Droplet-based synthetic method using microflow focusing and droplet fusion," *Microfluidics and Nanofluidics*, vol. 3, pp. 239–243, 2007.

[77] L.-H. Hung, K. M. Choi, W.-Y. Tseng, Y.-C. Tan, K. J. Shea, and A. P. Lee, "Alternating droplet generation and controlled dynamic droplet fusion in microfluidic device for cds nanoparticle synthesis," *Lab on a Chip*, vol. 6, no. 2, pp. 174–178, 2006.

[78] X. Niu, S. Gulati, J. B. Edel, and A. J. demello, "Pillar-induced droplet merging in microfluidic circuits," *Lab on a Chip*, vol. 8, no. 11, pp. 1837–1841, 2008.

[79] J. Sivasamy, Y. C. Chim, T.-N. Wong, N.-T. Nguyen, and L. Yobas, "Reliable addition of reagents into microfluidic droplets," *Microfluidics and Nanofluidics*, vol. 8, pp. 409–416, 2010.

[80] Y. Jang, C. Cha, J. Jung, and J. Oh, "Interfacial compression-dependent merging of two miscible microdroplets in an asymmetric cross-junction for in situ microgel formation," *Macromolecular Research*, vol. 26, no. 12, pp. 1143–1149, 2018.

[81] W.-H. Tan and S. Takeuchi, "Timing controllable electrofusion device for aqueous droplet-based microreactors," *Lab on a Chip*, vol. 6, no. 6, pp. 757–763, 2006.

[82] L. M. Diamante and T. Lan, "Absolute viscosities of vegetable oils at different temperatures and shear rate range of 64.5 to 4835 s- 1," *Journal of food processing*, vol. 2014, 2014.

[83] J.-C. Baret, "Surfactants in droplet-based microfluidics," *Lab on a Chip*, vol. 12, no. 3, pp. 422–433, 2012.

[84] M. Saqib, B. Ercan, and E. Y. Erdem, "Synthesis of anisotropic magnetic polymeric janus particles by in situ separation of magnetic nanoparticles in a microfluidic device," *Langmuir*, vol. 39, no. 48, pp. 17080–17087, 2023.

[85] J. Vuksanović, I. Radović, S. P. Šerbanović, and M. Kijevčanin, "Experimental study of the thermodynamic and transport properties of binary mixtures of poly (ethylene glycol) diacrylate and alcohols at different temperatures," *Journal of the Serbian Chemical Society*, vol. 80, no. 7, pp. 933–946, 2015.

[86] A. L. R. Costa, A. Gomes, and R. L. Cunha, "Studies of droplets formation regime and actual flow rate of liquid-liquid flows in flow-focusing microfluidic devices," *Experimental Thermal and Fluid Science*, vol. 85, pp. 167–175, 2017.

[87] P. Xue, Y. Wu, N. V. Menon, and Y. Kang, "Microfluidic synthesis of monodisperse pegda microbeads for sustained release of 5-fluorouracil," *Microfluidics and Nanofluidics*, vol. 18, pp. 333–342, 2015.

[88] D. Hernández-Cid, V. Pérez-González, R. Gallo-Villanueva, J. González-Valdez, and M. Mata-Gómez, "Modeling droplet formation in microfluidic flow-focusing devices using the two-phases level set method," *Materials Today: Proceedings*, vol. 48, pp. 30–40, 2022.

[89] J. M. Camacho and V. Sosa, "Alternative method to calculate the magnetic field of permanent magnets with azimuthal symmetry," *Revista mexicana de física E*, vol. 59, no. 1, pp. 8–17, 2013.

[90] "Magnetic fields of solenoids and magnets." https://www.mathworks.com/matlabcentral/fileexchange/71881-magnetic-fields-of-solenoids-and-magnets. Accessed: 2022-07-16.

[91] T. Tenforde, "Thermoregulation in rodents exposed to high-intensity stationary magnetic fields," *Bioelectromagnetics: Journal of the Bioelectromagnetics Society, The Society for Physical Regulation in Biology and Medicine, The European Bioelectromagnetics Association*, vol. 7, no. 3, pp. 341–346, 1986.

[92] A. Özkan and E. Y. Erdem, "Numerical analysis of mixing performance in sinusoidal microchannels based on particle motion in droplets," *Microfluidics and Nanofluidics*, vol. 19, no. 5, pp. 1101–1108, 2015.

[93] M. Y. N. Husna, C. H. Chong, V.-L. Wong, K. H. Cheah, and Y. K. Wan, "3d-printed pegda monolith with robust silane-grafted chitosan for enhanced textile wastewater treatment," *Journal of Environmental Chemical Engineering*, vol. 10, no. 6, p. 108581, 2022.

[94] A. youhei, H. Hirotada, and T. Toru, "Hyper-miniaturisation of monodisperse janus hydrogel beads with magnetic anisotropy based on coagulation of fe 3 o 4 nanoparticles," *Journal of Materials Science and Chemical Engineering*, vol. 1, no. 02, pp. 1–5, 2013.

Appendix A

Fabrication Methods

Making a SU8 mold consists of two major steps, one is the base layer coating which acts as an adhesive. The second step is the main layer coating that will hold the pattern.

A.1 Cleaning Process

Rinse the polished silicon wafer with acetone and without letting the acetone depart the surface rinse the wafer with IPA. Finally rinse it with DI water and blow drying with N_2. After drying the wafer place it in dehydration oven at 120 C for at least five minutes to allow all the moisture to be removed from the surface.

A.2 Base Layer

While the wafer is being heated up in the dehydration oven, prepare to set up two hot plates in close proximity to each other on a workbench, one at 65 C and the other at 95 C.

A.2.1 Spin coating for base layer

After removing it from the oven allow the wafer to cool uniformly to room temperature by placing it on an insulating surface preferably on a few layers of cleanroom wipes. While the wafer cools, you may set the spin parameters for the base coating which are shown in Table

Table A.1: Spin coating steps for base layer of SU8 2005

Step	Velocity (rpm)	Acceleration (rpm/s)	Time (s)
1	500	100	25
2	2500	200	40

Before getting started with the spin process, make sure that the spinner is covered in Al foil from inside. Using the specially provided gauge, mount the wafer on to the chuck and apply vacuum. Just to be sure of the vacuum and availability of the spinner, run the process with the plain wafer. After that pour around $4ml$ of SU 8 2005 on to the center of the wafer and start spinner. Continuously monitor spinner parameters and the wafer surface and make sure the step is fully executed. While the program will be running it will display *running* and when it finishes successfully it will display *done*.

A.2.2 Pre-bake for the Base Layer

As soon as the spinning is done, open the lid of the spinner and turn off vacuum and remove the wafer and place it on a piece of Al foil around 8 by 8 inch (it will facilitate the transportation of the sample) and immediately proceed to start the pre-bake process.

Make arrangements to strictly follow the time intervals using a timer and a pair of active hands.

Table A.2: Soft bake steps for base layer of SU8 2005

Step	Temperature (°C)	Time (min)
1	65	2
2	95	4
3	65	1

A.2.3 Exposure for Base Layer

Exposure should be done after allowing the wafer to cool to room temperature again as mentioned before in the spin coating section. The details of the process are

- Manual top side
- Contact mode = soft contact
- Separation = 100μm
- Mask thickness = 2.3mm
- Sample thickness = 0.5mm
- Resist thickness = 2μm
- Exposure intensity = $120mJ/cm^2$.

A.2.4 Hard Bake for the Base Layer

After the exposure proceed again to the work bench and start post bake after exposure.

Again allow it to uniformly cool down to room temperature.

Table A.3: Hard bake steps for base layer of SU8 2005

Step	Temperature (°C)	Time (min)
1	65	1
2	95	3
3	65	1

A.3 Main SU8 layer

Now you can proceed with the recipe for the main SU 8 2050 that will contain the pattern.

A.3.1 Spin coating for second layer

Set the spin parameters for the second coating which are

Table A.4: Spin coating steps for main mold layer of SU8 2050

Step	Velocity (rpm)	Acceleration (rpm/s)	Time (s)
1	500	50	40
2	2200	300	35

Before getting started with the spin process, make sure that the spinner is covered in Al foil from inside. Using the specially provided gauge, mount the wafer on to the chuck and apply vacuum. Just to be sure of the vacuum and availability of the spinner, run the process with the plain wafer. After that pour around 4ml of SU 8 2050 on to the center of the wafer and start spinner. Continuously monitor spinner parameters and the wafer surface and make sure the step is fully executed. While the program will be running it will display *running* and when it finishes successfully it will display *done*. As soon as the spinning is done, open the lid of the spinner and start the edge removal process by using a glass slide and using its corner to nicely and smoothly remove SU8 from the edges of the circular wafer. Just watch out for any falling SU 8 drops from the lid as you do this. Now turn off vacuum and place wafer on a piece of

Al foil around 8x8 inch (it will facilitate the transportation of the sample) and immediately proceed to start the prebake process.

A.3.2 Pre bake for the second layer

Table A.5: Soft bake steps for main mold layer of SU8 2050

Step	Temperature (°C)	Time (min)
1	65	3
2	95	8
3	65	2

Make arrangements to strictly follow the time intervals using a timer and a pair of active hands.

A.3.3 Exposure for second layer

Exposure should be done after allowing the wafer to cool to room temperature again as mentioned before in the spin coating section. The details of the process are

- Manual top side
- Contact mode = soft contact
- Separation = 200μm
- Mask thickness = 2.3mm
- Sample thickness = 0.5mm
- Resist thickness = 2μm
- Exposure intensity = $230 mJ/cm^2$.

A.3.4 Post exposure bake for second layer

After the exposure proceed again to the work bench and start post bake after exposure.

Table A.6: Hard bake steps for main mold layer of SU8 2050

Step	Temperature (°C)	Time (min)
1	65	3
2	95	8
3	65	2

A.3.5 Development for the SU 8 mold on the wafer

After allowing the wafer to cool to room temperature at a uniform rate, proceed to the workbench and pour around as much developer in a beaker as would completely drown the wafer but do not over use. Place the wafer into the beaker and then start agitating the beaker very slowly and carefully. Too much agitation might cause damage to the pattern and too less might result in developer not reaching certain corners and gaps. After around 9 minutes of development take out the wafer from the beaker and immediately rinse it with thoroughly with IPA and then with water, dry it and observe the pattern. If there are some SU 8 residual marks on the wafer, then use another development step but use fresh developer and only develop for a 30 seconds or so. Again repeat the cleaning and drying steps. You will observe that the pattern is now clean and accurately defined on the wafer.

Appendix B

Experimental Procedure

B.1 Making PDMS Mold

Polydimethylsiloxane $PDMS$ (Sylgard silicone elastomer, Dow Corning GmbH, Germany) was made by adding the polymer and curing agent in a ratio of 10:1 and mixing steadily for a period of 2-3 minutes. Then the PDMS was poured onto the SU8 master mold contained in a petri dish. By using vacuum degassing the bubbles were removed to ensure clear PDMS mold. Afterwards, the PDMS was allowed to cure at a temperature of 80 C in an incubator for a period of 70-80 minutes.

After the curing process is completed, the excess PDMS is cut off from sides and the main PDMS mold is peeled off the Si wafer. The devices are cut using cutters and covered with scotch tape to protect against contamination while the bonding process starts.

B.2 Bonding PDMS

The PDMS mold post-processing includes the punching of holes using a 5 mm puncher in the inlet and outlet ports. Following the punches of holes, the PDMS mold was cleaned by rinsing with IPA and deionized water and then dried with N_2. For the base, a clean piece of PDMS is used.

Using Exposure Power = 150 W, the PDMS mold and glass slide were exposed to Oxygen Plasma in a Plasma Cleaner to obtain free surface and then bonded to each other by mating the free surfaces of PDMS and the glass slide. After bonding, the device was sealed at the sides with epoxy to prevent and leakage and then the inlet plastic capillary tubing was fixed and the circumference of the tubing at the inlet sealed with epoxy to prevent any leakage of fluid.